# Whistler Wave Interaction with a Density Striation: A Laboratory Investigation of an Auroral Process

J. F. Bamber, J. E. Maggs, and W. Gekelman

*Department of Physics, University of California,*

*Los Angeles, California 90095*

Whistler waves are launched toward a field-aligned density striation in a laboratory plasma. Characteristic scale length and frequency ratios are scaled to closely reproduce situations found in the auroral ionosphere. Detailed measurements show that at the striation edge nearest the wave-launching antenna, besides a reflected and a transmitted whistler wave, lower hybrid waves are also stimulated on both sides of the striation boundary in a manner consistent with the linear mode-conversion model. We find that the energy density of the mode-converted lower hybrid waves is typically 10% of the incident whistler wave energy density, reaching a maximum of 30% in one region. Lower hybrid waves are confined to within 2-3 perpendicular wavelengths in the interaction zone. Our results show that the interaction of electromagnetic whistler mode waves with density striations can cause significant amounts of energy to be deposited in the largely electrostatic lower hybrid mode and that it may, therefore, be a significant generation mechanism for these waves in certain regions of the ionosphere.

## Introduction

The investigation of the behavior of electromagnetic whistler waves in the vicinity of a field-aligned density striation is motivated by a number of observations made in the near-earth environment. First, these waves are commonly found in almost all parts of the magnetosphere and ionosphere [*Helliwell*, 1965; *Walker*, 1976; *Shawhan*, 1979; *Al'pert*, 1980, 1983; and *Carpenter*, 1983]. Second, at altitudes below approximately 5000 km, the high latitude ionospheric plasma is found to contain short scale-length, field-aligned irregularities or striations [*Herman*, 1966; *Dyson*, 1969; *Clark and Raitt*, 1976; *Kelley and Mozer*, 1972; *Fejer and Kelley*, 1980] at all accessible altitudes and all local times. The striations are almost always of lower density than the background and the density amplitude distribution peaks between 10% and 30% of the background level [*Dyson*, 1969]. It is generally believed that the size of the striation parallel to the background magnetic field is very large compared to its extent across the field so that the shape is either cylinder-like or sheet-like. The cross-field dimension ranges from as small as 10 m to hundreds of km. Although striations are basically a high-latitude phenomenon, with most observations being made at $L \geq 4$ (invariant latitude $|\Lambda| \geq 60°$), there is also a small region where striations exist near the magnetic equator, $|\Lambda| \leq 20°$ [*Kelley and Mozer*, 1972]. Clearly, whistler waves propagating in these regions must frequently encounter density striations. The electromagnetic whistler wavelength in the topside ionosphere is on the order of 1 km. Measurements with very high spatial resolution made in the ionosphere below 1000 km, on a series of rocket flights [*Vago et al.*, 1992], directly show the existence of the small-scale density striations which are typically 100 m across (minimum 10 m) with an average spacing of ~1 km. It

is the interaction of whistler waves with this type of short perpendicular scale length striation that is the topic of this paper.

Early observations, beginning in the 1960's, typically deal with whistler wave interactions with irregularities having cross-field dimensions much greater than the whistler wavelength. The observed phenomena are generally characterized by refraction [*Carpenter*, 1968; *Smith and Angerami*, 1968; *Cerisier*, 1974]. However, a series of experiments performed in the 1980's, extends the observations to the opposite regime where the striation width is less than the whistler wavelength. The key experiments were performed in October 1980 — January 1981 as reported by Bell et al. [*Bell et al.*, 1983; *Bell and Ngo*, 1988, 1990]. These authors examine signals launched by a number of large transmitters located in the United States, Antarctica, and elsewhere, which are detected by satellites at low altitude (600-3800 km). The signals are in the whistler frequency range and normally produce electromagnetic whistler waves in the ionosphere. However, during conditions where the lower hybrid resonance (LHR) noise shows an irregular lower cutoff frequency, indicating the presence of density striations, they find that the signals, transmitted with a bandwidth of ~1 Hz, can undergo considerable spectral broadening (up to 2 kHz) as detected by an electric dipole probe. Several important characteristics of the phenomenon lead to the conclusion that the broadening is caused by the appearance of much shorter wavelength lower hybrid waves which are Doppler-shifted in the spacecraft frame of reference. These characteristics include the dependence on antenna orientation, cutoff at the LHR frequency, the chevron shaped frequency-time envelope, and the manner in which the broadened signals are modulated by the spacecraft spin [*James and Bell*, 1987]. It should be pointed out that this phenomenon is not limited to whistler waves artificially injected into the ionosphere but may also

occur with natural whistler wave radiation. The naturally occurring interaction is, however, much more difficult to detect given the broad frequency spectra of the natural waves.

A number of mechanisms have been proposed to explain the appearance of the lower hybrid waves, but we focus upon only the one which appears most likely, and is also the simplest, namely linear mode-coupling (also referred to in the literature as passive linear mode-coupling, direct conversion, passive linear scattering, or simply linear scattering). The idea was introduced by *Piliya* [1966] who suggested that it would be possible to couple two allowed modes in a plasma by means of some type of spatial gradient. In this process there is no requirement of an amplitude threshold, as in the case of parametric instabilities. The efficiency is determined only by the steepness of the gradient. Application of the direct conversion idea to the situation of interest in this work can be described, briefly, as follows. Incident electromagnetic whistler waves scatter from field-aligned density striations whose perpendicular gradient scale length is much shorter than the perpendicular whistler wavelength, generating lower hybrid waves essentially by reflection from a sharp interface [*Bell et al.*, 1983; *Bell and Ngo*, 1988, 1990]. The parallel wavenumber, $k_{\|}$, is provided by the incident whistler wave. At a given $k_{\|}$, multiple values of $k_{\perp}$ are allowed by the dispersion relation. A broad spectrum of perpendicular wavenumbers, $\Delta k_{\perp}$, is provided by the striation. This spectrum of $\Delta k_{\perp}$ values allows the jump from one mode to the other. It is important to note that the spectrum is limited by the steepness of the gradient. The smoother the gradient, the smaller the gap which can be bridged in $k_{\perp}$.

For frequencies between the lower hybrid resonance and half the electron cyclotron frequency, $f_{LH} < f < f_{ce}/2$, the cold plasma dispersion relation allows

up to four values of $k_\perp$ for any $k_\parallel$ corresponding to a whistler wave. Thus, the incident wave potentially can linearly couple to one whistler and one lower hybrid mode inside, and one whistler and one lower hybrid mode outside the striation. At present there are no observations, in space or in the lab, which are inconsistent with this model. On the other hand, linear mode-coupling has never been *directly* observed. The main result of the current work is the direct observation of the mode-conversion of whistler waves to lower hybrid waves at a density striation. This observation is significant not only in establishing a basic plasma physics process which commonly occurs in the ionosphere, but also in its relation to another topic of much interest recently; that is, the problem of ion heating in the ionosphere. Many authors believe that ion heating can be caused by lower hybrid waves [*Chang*, 1993]. Recently, *Kintner et al.* [1992] and *Vago et al.* [1992] have found a direct correspondence between lower hybrid wave activity and perpendicular ion acceleration in the vicinity of density striations in the topside auroral ionosphere. Although the observed lower hybrid waves may or may not arise from mode-converted whistler waves in this particular region, these observations indicate that lower hybrid waves created in any manner are able to cause transverse ion energization.

Previously we stated that this was the first direct observation of whistler wave mode-conversion at a density striation, either in space or in the lab. This should not be taken to imply that laboratory research on whistler waves has been lacking. Experimentation on whistler waves has quite a long history. The first laboratory experiment to successfully create and detect whistler mode waves was performed by *Gallet et al.* [1960]. This and other experiments in the decade of the 1960's concentrated on confirming such basic whistler properties as polarization, attenuation, and wavelength dependence on

frequency in plasmas with essentially uniform density. The most complete work has been performed by *Stenzel* [1975, 1976a, 1976b, 1976c]. In his fundamental work, *Stenzel* [1976a] establishes all the basic whistler properties including the dispersion (frequency vs. parallel wavenumber, $\omega$ vs. $k_{||}$), polarization, and group velocity over a large range of wave frequencies (mostly $\omega > \omega_{ce}/2$) and plasma parameters in a uniform plasma. As well, he goes on to measure the phase and amplitude distribution of the antenna radiation pattern in both uniform and slowly-varying plasmas. In the nonuniform case, refraction is observed as well as ducting in a density trough. Stenzel's work in slowly-varying plasma was extended by Sugai and coworkers [*Sugai et al.*, 1978a, 1978b, 1979, 1980]. From the early 1980's laboratory research on whistler waves has continued but in directions that are not relevant to this discussion. However, it is important to emphasize that, to date, there has not been any laboratory work reported on whistler wave propagation in a plasma containing short scale-length density variations. Thus, the present work represents an important extension of laboratory whistler wave research into areas previously unexplored.

## Description of Experiment

In this section we first briefly describe the experimental device as well as the measurement probes and wave-launching antenna used; after this we discuss of the details of the experiment itself. Our work is carried out in a machine designed to study space plasma physics phenomena. The LAPD (LArge Plasma Device) at UCLA [*Gekelman et al.*, 1991; *Pfister et al.*, 1991] is a flexible and low maintenance device suitable for studying a variety of waves

and nonlinear effects in fully magnetized plasmas. A photograph of the machine is shown in Plate 1.

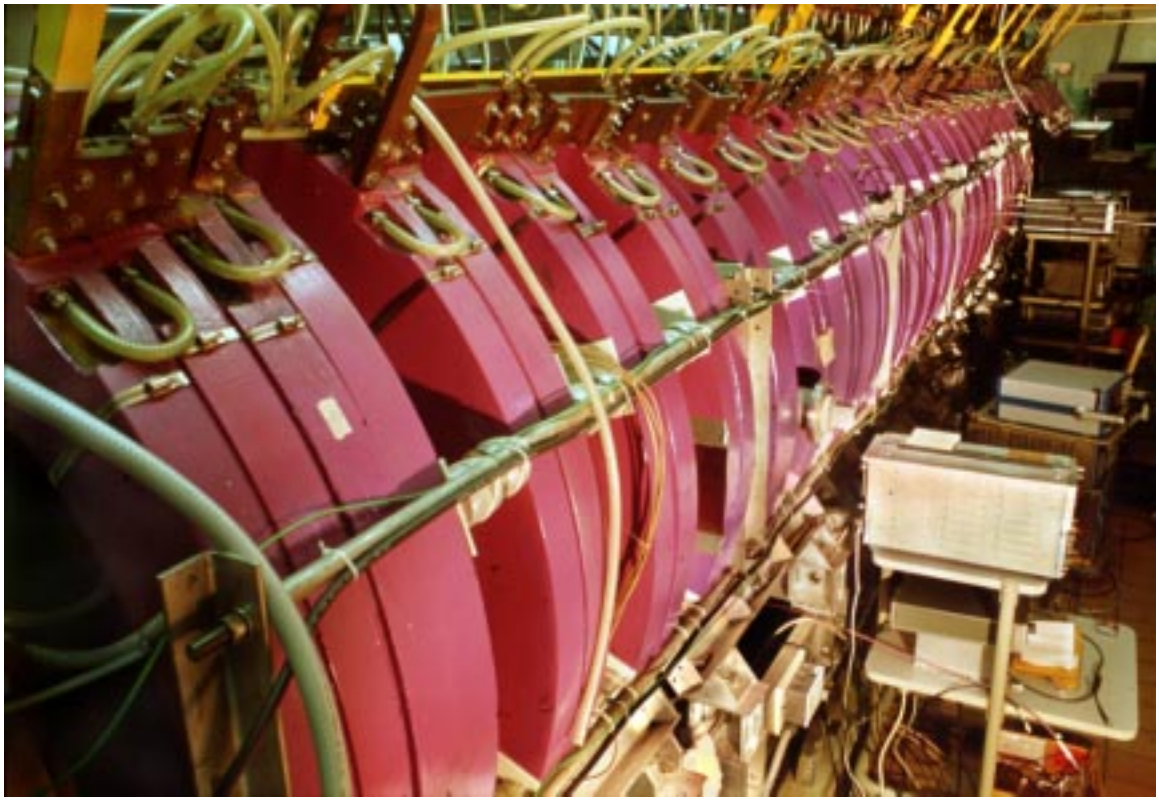

**Plate 1.** Photograph of the Large Plasma Device (LAPD) at UCLA. Visible in this photograph are the 68 magnet pairs which surround the 10 m long, 1 m diameter plasma chamber. Power and cooling water for the magnets are fed in from above. The cathode, which produces the DC discharge plasma, is located inside the far end of the machine. The plasma is accessible to probes through ports between the magnet pairs.

The vacuum chamber is 10 m in length and 1 m in diameter and is surrounded by 68 magnet coils. Within the chamber, the plasma column has a diameter of up to 80 cm along the full 10 m length. As viewed in Plate 1, the coordinate system is defined with $x$ pointing to the right, $y$ pointing upward, and $z$ pointing toward the viewer along the axis of the machine. The axial

magnetic field ranges from 10 to 3000 G and is independently adjustable in 7 sections along the length of the machine. This configuration allows for a variety of magnetic field profiles from uniform to mirror geometry. The plasma is produced by a DC discharge driven by a barium oxide coated nickel cathode which is pulsed negative with respect to a grid anode placed some distance (~0.5 m) along the plasma chamber. The oxide coating reduces the work function of the cathode so that it may emit ionizing electrons at reasonably low temperatures (*i.e.* 900° C). The discharge is pulsed on approximately once per second with the plasma lasting typically several ms.

The plasma is created along the full length of the machine. At appropriate neutral gas pressures ($\leq 5\times10^{-4}$ Torr, helium), the axial density gradient is negligible except very near the end of the machine opposite the cathode. The density drops approximately 3% per meter for the bulk plasma. Densities increasing from $2\times10^{11}$ cm$^{-3}$ to $5\times10^{12}$ cm$^{-3}$ can be obtained by increasing the discharge voltage, heater temperature, and/or neutral gas pressure. Density fluctuations from shot to shot are on the order of 1% in the center of the plasma column and increase to ~5% in the outer edge region where the plasma density begins to fall off.

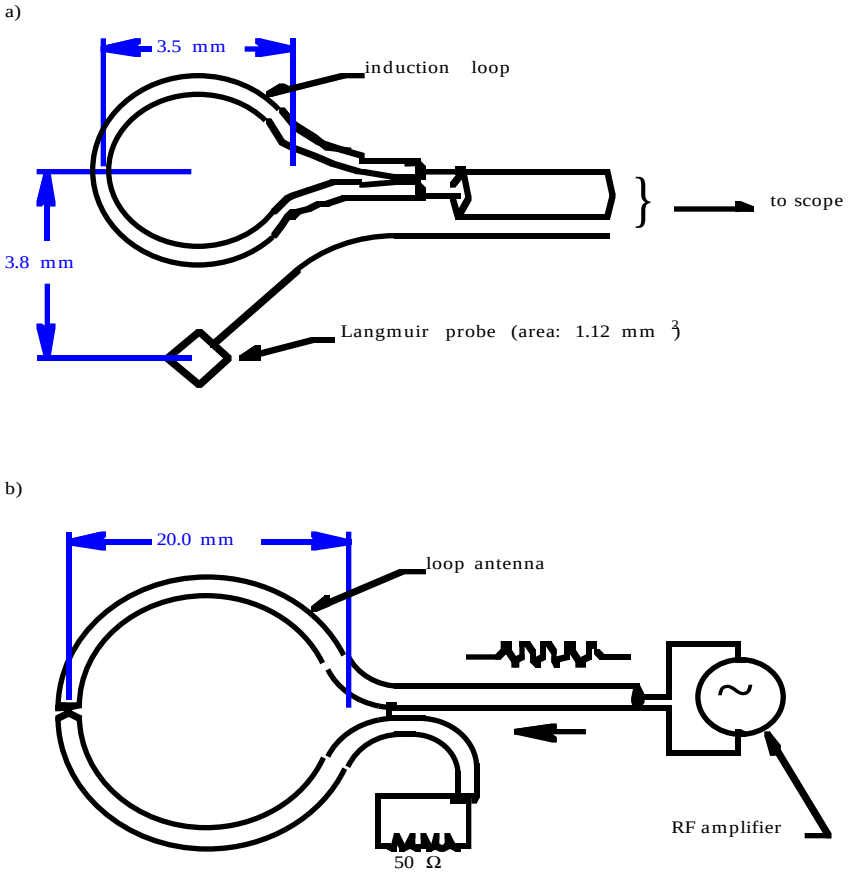


**Figure 1**

**Figure 1.** Schematic drawings of the measurement probe and wave-launching antenna. The probe (a) comprises an induction loop and a Langmuir probe. The induction loop is a single turn loop with a diameter of 3.5 mm constructed from coaxial cable. A voltage is induced along the inner wire by oscillating magnetic fields; the outer conductor provides shielding. The voltage signal is transmitted out of the chamber on another coaxial cable. Several other shielding and insulating layers on the induction loop and signal cable, required to minimize pickup noise as much as possible, are not shown. The Langmuir probe is simply the flattened, exposed end of an insulated wire with a total exposed area of 1.12 $mm^2$. The antenna (b) is a single turn loop

constructed from coaxial cable. Note that the antenna is much larger than the induction loop with a diameter of 20.0 mm. The current path through the antenna, beginning on the inner conductor, goes around the loop, over the 50 Ω load onto the outer conductor, back to the base of the loop where it cuts across and returns to the amplifier. Thus, the only region where the current does not flow coaxially is around the loop itself. An insulating layer, not shown, prevents any electrical contact with the plasma

The probe used for this experiment is shown in Fig. 1(a). It comprises a magnetic induction loop and a Langmuir probe. The relative plasma density profile is derived from the current-voltage characteristics of the Langmuir probe using standard techniques [*Chen*, 1965]. Absolute scaling of the density is obtained by comparison of the measured antenna radiation pattern measured in a region of uniform plasma density with patterns calculated using a Green's function analysis for our particular antenna in a cold, uniform, unbounded plasma (the Green's function analysis is discussed below). Calculations are made for a series of density values. We estimate the absolute density values obtained using this method to be accurate within ±10%.

The parallel component of the oscillating magnetic field, $B_z$, is obtained from the induction loop signal [*Lovberg*, 1965]. Our experiments have two particular requirements: 1) small probe size to resolve the short wavelength lower hybrid waves and 2) extremely good shielding because of the high frequencies involved (~100 MHz) and the small signals expected. In the work described in this paper, all of the measurements are made locally; that is, the probe is placed at a certain $(x, y, z)$ location and, during a specified time period in the discharge, data are measured and stored. Each measurement is repeated, at a single location, for a number of pulses in order to form an

average. The resulting time series is considered to represent the corresponding field variable at that location and over that period of time. The whole process, repeated over all of the spatial locations, forms an ensemble allowing one to see a spatial picture of the phenomena under investigation. At each location, the repeated measurements show that typically 90% of the $B_z$ values lie within 5% of the mean value. Further, uncertainty in the determination of the probe area is within ±5%. Therefore, the overall uncertainty in the $B_z$ data is estimated to be ±10% for the typical observed amplitude. This uncertainty increases as the amplitude of the $B_z$ data decreases to the level of the background noise.

The incident whistler wave is launched by a 2 cm diameter loop antenna, shown schematically in Fig. 1(b). The loop is completely insulated from the plasma in order to ensure purely inductive coupling. It is oriented with its normal parallel to the background magnetic field, $\mathbf{B}_0$. The size and inductive nature of the antenna allow it to couple efficiently to electromagnetic whistler waves. Conversely, lower hybrid waves, which have a reduced magnetic field component and a short wavelength perpendicular to $\mathbf{B}_0$ (less than the loop diameter as discussed below), are not excited to any significant degree by the antenna. This is shown by the fact that they could not be detected in earlier experiments involving a uniform plasma with no density striation.

Our experiments are performed in a Helium plasma column with a static background magnetic field strength of $B_0 = 480$ G. The plasma has a bulk density of $n_e \approx 9\times10^{11}$ cm$^{-3}$ containing a field-aligned cylindrical striation with a minimum density of $3\times10^{11}$ cm$^{-3}$. The diameter of the striation, $d$, across the plasma is approximately 6 cm. The diameter of the entire plasma column is 80 cm. A contour plot of the plasma density in a plane perpendicular to $\mathbf{B}_0$ along with a perpendicular scan through the center of the

striation are shown in Fig. 2. The striation can clearly be seen.

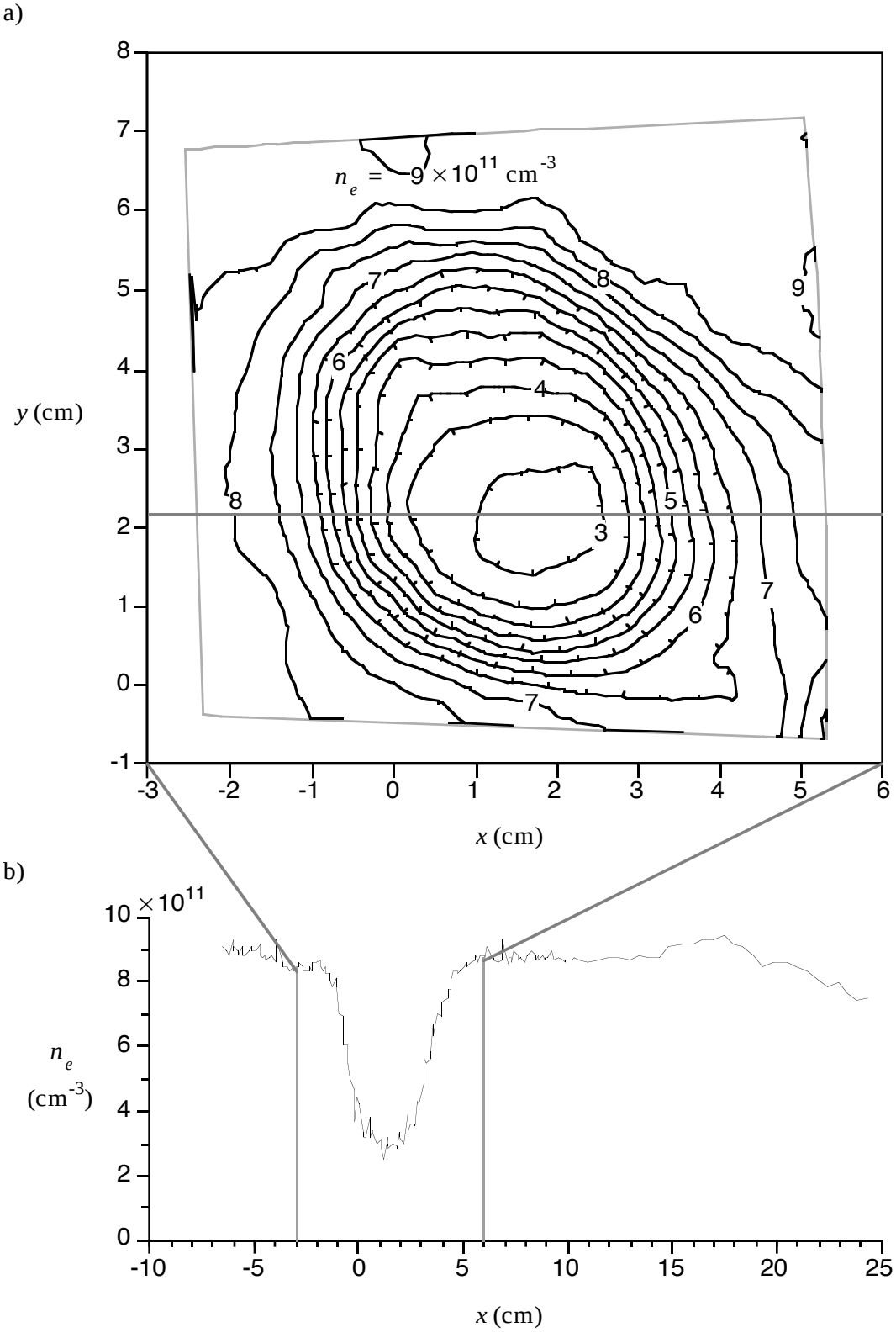


**Figure 2**

**Figure 2.** Plasma density in the vicinity of the striation. Density contours (a) in a plane perpendicular to the background magnetic field are shown in the immediate vicinity of the striation. A scan along *x* through the center of the striation, and extending into the bulk plasma where the whistler waves propagate, is shown in (b). The *y*-location of the scan is indicated in (a) by the dotted horizontal line. It can be seen that the density gradient is quite steep, having a minimum scale length of 1.5 cm, which is on the order of 0.1 of the perpendicular whistler wavelength. Small discrepancies between the data in (a) and (b) are due to measurements having been made under slightly different plasma conditions.

These measurements are made over 6 m from the cathode. In fact, we observe the density profile to remain almost unchanged at all *z*-locations up to ~9 m away from the cathode. The density gradient is very sharp; the minimum gradient scale length, $L_\nabla \equiv N_e / \nabla N_e$, is 1.5 cm. This is on the order of 0.1 of the perpendicular whistler wavelength. Thus, the edge of the striation may be considered to approximate a sharp interface with respect to the incident whistler wave. The striation is produced by leaving a circle in the center of the cathode free of the barium oxide coating. Primary electrons are not emitted from this region and, thus, no ionization from primary electrons occurs along magnetic field lines connected to it.

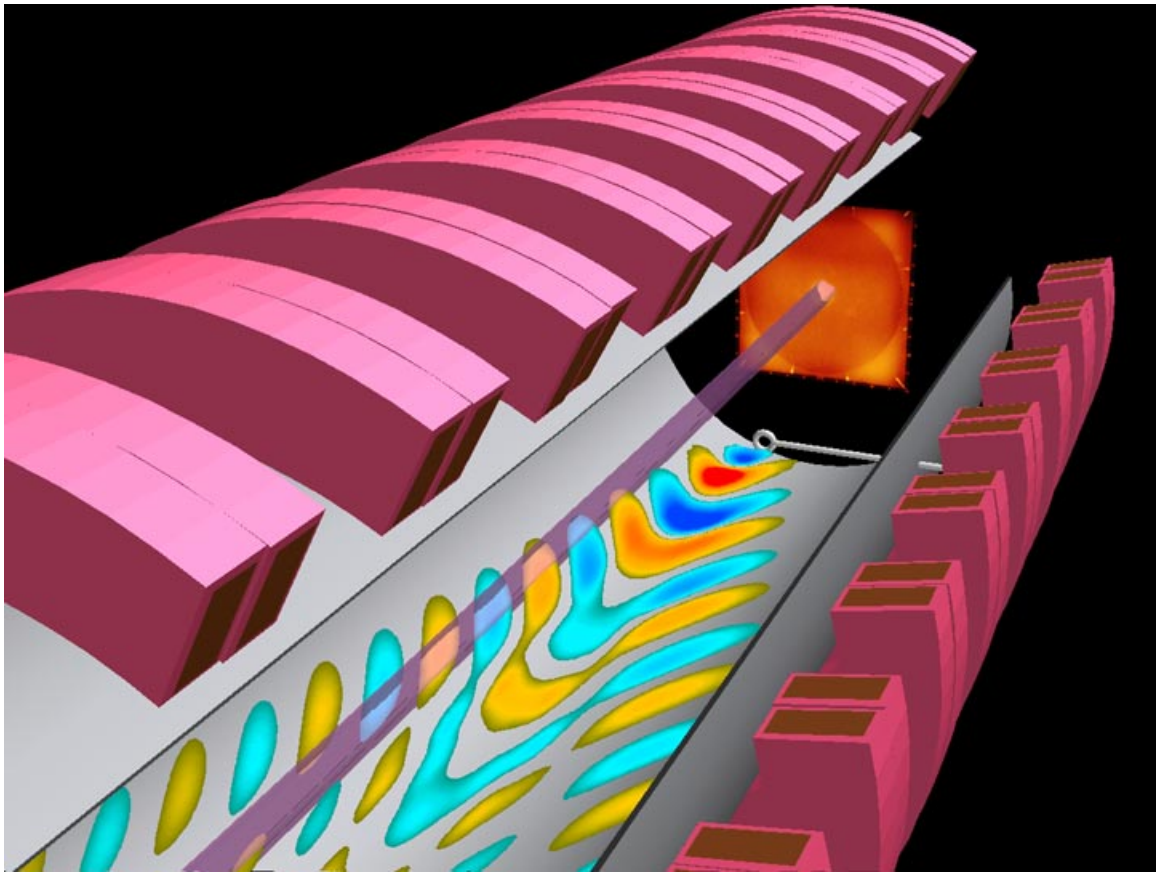

**Plate 2.** Schematic, to scale, representation of the whistler wave – striation interaction experiment. The striation, depicted by the purple cylinder, is located along the central axis of the machine. Whistler waves are launched from an antenna which is inserted into the machine slightly below the midplane to within 1 perpendicular whistler wavelength of the striation. The antenna radiation pattern, shown in blue and yellow, is calculated for an infinite, homogeneous, cold plasma using a Green's function analysis based on our actual antenna. This pattern, it should be stressed is the expected pattern in the absence of the striation. The radiation first impinges upon the striation approximately 2 parallel wavelengths downstream from the antenna. This region features the strongest interaction because the wave amplitude is highest here; therefore, our experiments focus on this region.

The placement of the antenna with respect to the density striation is illustrated in plate 2. Also shown in this schematic representation is the antenna radiation pattern, calculated for a uniform plasma, in a plane transecting the striation. The signal applied to the antenna is a single-frequency sine wave with an amplitude such that ~2 A flows through the antenna circuit at a frequency of $f$ = 101 MHz. For comparison, the electron cyclotron frequency is $f_{ce}$ = 1.3 GHz, the plasma frequency is $f_{pe}$ = 8.5 GHz, and the lower hybrid resonance frequency is $f_{LHR}$ = 15 MHz The wave magnetic fields in the vicinity of the striation are on the order of 100-200 mG. The antenna is placed 10 cm from the edge of the striation. In terms of scaled parameters, this distance is slightly less than one perpendicular whistler wavelength (how this and other wavelengths in our experiment are obtained is discussed in detail below). The radiation, it is seen, is constrained to lie within a cone, the angle of which is defined by the maximum ray angle (~18° for our experiment). Thus, the interaction takes place in a region at the striation edge 30 cm away from the antenna, in the parallel direction. This distance corresponds to ~2 parallel whistler wavelengths. Mode-converted lower hybrid waves, from the cold plasma dispersion relation, are expected to have a perpendicular wavelength, $\lambda_{\perp,LH}$, of 1.4 cm. The three key parameters, $B_0$, $n_e$, and $f$, are chosen to provide the best wavelength and frequency scaling as compared to typical conditions in the ionosphere, subject to experimental constraints. This is illustrated in Table 1 which summarizes the important quantities and ratios, both in the LAPD and in the ionosphere at 1000 km.

TABLE 1. Typical whistler wave – striation interaction parameters and ratios in the ionosphere and the LAPD

| parameter | ionosphere (~ 1000 km) | LAPD | ratio | ionosphere (~ 1000 km) | LAPD |
|---|---|---|---|---|---|

| | | | | | |
|---|---|---|---|---|---|
| $f$ | 5-30 kHz | 101 MHz | $f/f_{LH}$ | 1-7 | 6.7 |
| $f_{LH}$ | 4.5-6 kHz | 15 MHz | $f/f_{ce}$ | 0.005-0.030 | 0.077 |
| $f_{ce}$ | 1 MHz | 1.3 GHz | $f_{pe}/f_{ce}$ | 0.6-1.0 | 6.5 |
| $f_{pe}$ | 0.6-1 MHz | 8.5 GHz | $d/r_{ci}$ | 2-150 | 15 |
| $r_{ci}$ | 6.5 m | 0.4 cm | $d/L_{\nabla}$ | 1-10 | 4.6 |
| $d$ | 10-1000 m | 6 cm | $\lambda_{\|}/d$ | 1-650 | 2.7 |
| $L_{\nabla}$ | 10-300 m | 1.3 cm | $\lambda_{\|}/L_{\nabla}$ | 2-650 | 12.3 |
| $\lambda_{\|}$ | 0.5-6.5 km | 16 cm | $\lambda_{\perp,LH}/L_{\nabla}$ | 0.1-3.5 | 1.1 |
| $\lambda_{\perp,LH}$ | 20-35 m | 1.4 cm | $\lambda_{\|}/\lambda_{\perp,LH}$ | 15-300 | 11 |

## Theory

The cold plasma dispersion relation in our experimental parameter regime, valid for the frequency range ($\omega_{LHR} \le \omega << \omega_{ce}, \omega_{pe}$) can be approximated by:

$$n^2 = 1 - \frac{\left(\omega_{pe}^2/\omega\right)}{\omega - \omega_{ce}\cos\theta} \ . \qquad (1)$$

where $n = \left[n_{\perp}^2 + n_{\|}^2\right]^{1/2} \equiv \frac{ck}{\omega}$ is the index of refraction, $c$ the speed of light, $k$ the wave-vector magnitude, $\theta$ the angle **k** makes with $\mathbf{B}_0$, and $\omega$ the angular frequency. The dispersion relation (1) gives rise to both whistler waves and lower hybrid waves. There is no sharp distinction between these modes; the whistler gradually transforms into the lower hybrid mode as the propagation angle approaches the resonance cone angle for propagation (the angle where $\omega = \omega_{ce}\cos\theta$) *Helliwell* [1965]. Figure 3 shows a plot of the wave normal curve

($k_{\|}$ vs. $k_{\perp}$) for two different plasma densities but the same magnetic field and wave frequency.

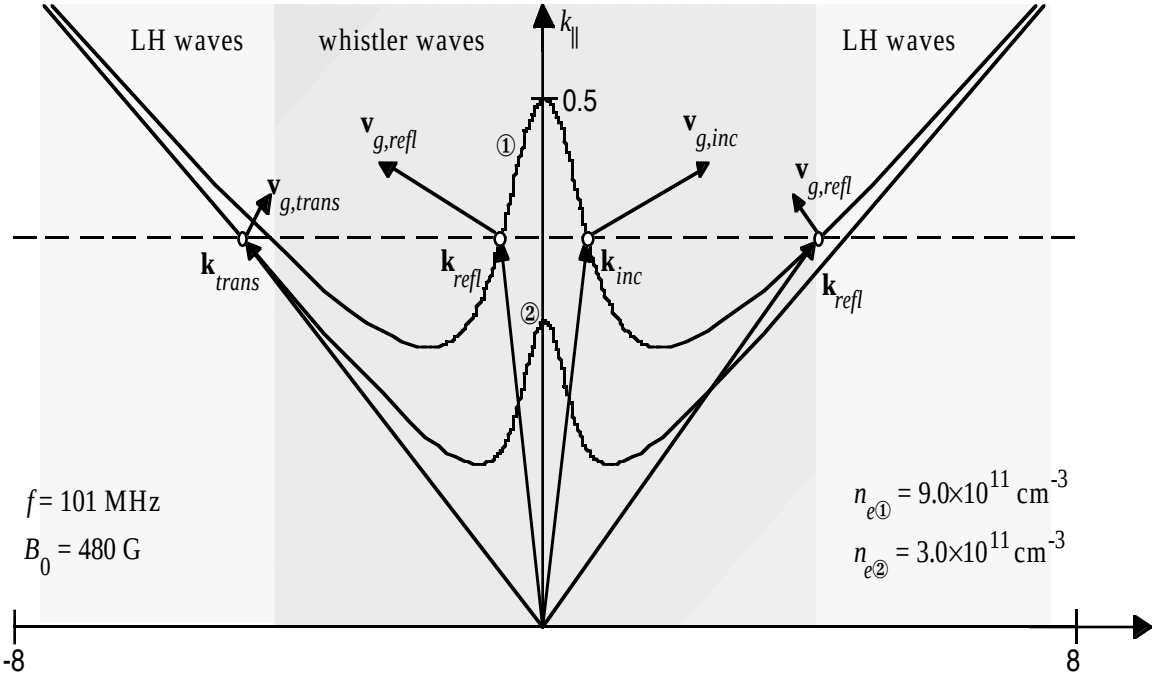


**Figure 3.** $k_{\|}$ vs. $k_{\perp}$ for two different plasma densities. The range of propagation angles is divided into a whistler wave section and a lower hybrid wave section. These sections are separated at the point of minimum $k_{\|}$. The two curves represent two adjacent regions of plasma. The first region has a density 3 times the density of the second. These two regions meet at a boundary whose normal is perpendicular to the background magnetic field. A whistler wave, propagating to the right, with wave vector $\mathbf{k}_{inc}$, is incident upon this boundary. A number of new waves, having the same parallel wavenumber as the incident wave, are generated (subject to the group velocity being in the appropriate direction). In this case, there is a reflected whistler wave as well as lower hybrid waves radiating away from both sides of the boundary. The transmitted whistler wave mode is evanescent. The

various wave and group velocity vectors associated with each wave are indicated on the figure.

The scale of the plot is expanded in the parallel direction to bring out detail. Whistler waves, electromagnetic in nature, are defined as those with **k**-vectors lying in the central region, between the points of minimum $k_{\|}$ (the darker shaded region). Lower hybrid waves, or "electrostatic whistlers", lie outside of the points of minimum $k_{\|}$ (the lighter shaded regions), and are basically electrostatic with their electric field very nearly aligned with the wave-vector.

Consider the situation where a plasma contains a high density region, with corresponding wave normal curve labeled ① in Fig. 3, bordering a low density region, with curve labeled ②. Suppose an incident plane electromagnetic whistler wave, with wave vector $\mathbf{k}_{inc}$, propagates toward the right, from the higher to the lower density region. The boundary between the two regions is field-aligned (*i. e.* its normal is perpendicular to the field) and its width is much less than the wavelength of the incident wave. This situation is the one-dimensional equivalent of our experimental situation. As the incident wave impinges upon the boundary, new waves are generated on both sides of the boundary. These waves are subject to the condition that they have the same $k_{\|}$ as the incident wave (indicated by the dashed line in Fig. 3). In turn, the possible values of $k_{\perp}$ are fixed via the dispersion relation, equation (1). In general, two reflected and two transmitted waves may be generated, one pair of whistler waves and one pair of lower hybrid waves. In our case, as illustrated in Figure 3, the transmitted whistler wave is evanescent since the dashed $k_{\|}$ line does not intersect the whistler portion of the region ② wave normal curve. The amplitudes of the waves corresponding to the values of $k_{\perp}$ which satisfy the dispersion relation are determined in part by the steepness

of the density gradient at the boundary. The density gradient acts as a source; therefore, the convolution integral of its $k_\perp$-spectrum with the $k_\perp$-spectrum of the incident whistler gives the source strength as a function of $k_\perp$. This function must be broad enough to include the lower hybrid wave $k_\perp$ values if mode-conversion is to occur.

The group velocity direction of each wave is shown by the arrows perpendicular to the curves. Note that the whistler waves shown here propagate at ~50° to the background magnetic field with group velocities ~15°. These angles are not truly represented in Fig. 3 because the axes do not have the same scale. The lower hybrid waves are "backwards-propagating" perpendicular to the magnetic field. That is, their phase fronts propagate toward the interface (almost perpendicular to $\mathbf{B}_0$) but their group velocity (mainly along $\mathbf{B}_0$) has a small perpendicular component away from the interface. Of course, a single planar interface presents a simpler case than that of either sheets or filaments as observed in the ionosphere and magnetosphere. *Bell and Ngo* [1990] also model a smoother density profile using multiple planar interfaces. No equivalent theoretical work has been published for the case of a cylindrical striation. However, we assume that the basic concepts discussed here may be applied to a cylindrical geometry in a straightforward manner.

## Uniform Case

Before performing the whistler wave — striation interaction experiments described above, we first performed an experiment measuring the antenna radiation pattern in a uniform plasma. We wanted to determine: (a) whether lower hybrid waves appear in the uniform case and (b) whether the measured

antenna radiation pattern conforms to that calculated using a Green's function analysis based on a current loop source imbedded in an infinite, homogeneous, cold plasma. Briefly, the Green's function analysis begins as in the case of a single plane wave [*Stix*, 1962]. The difference lies in the inclusion of an external current source, $\mathbf{J}_A$, corresponding to the antenna which, in cylindrical coordinates, is given by

$$\mathbf{J}_A = I\delta(z)\delta(r - r_A)\hat{\phi}e^{-i\omega_0 t} \tag{2}$$

where $I$ is the total current flowing in the antenna loop and $r_A$ is the radius of the loop, assumed to be circular and of infinitesimal extent in the $r$ and $z$ directions. Plane wave dependence of the variables can not be assumed but we may restrict the time dependence to be monochromatic, $\exp(-i\omega_0 t)$. The resulting wave equation is

$$\nabla(\nabla\cdot\mathbf{E}) - \nabla^2\mathbf{E} - k_0^2\tilde{\varepsilon}\cdot\mathbf{E} = \frac{4\pi i}{\omega_0}k_0^2\mathbf{J}_A \tag{3}$$

where $\tilde{\varepsilon}$ is the dielectric tensor including damping due to collisions and the vacuum wavenumber, $k_0$, is employed to simplify the notation. To solve equation (3) one assumes that there exists a tensor Green's function, $\tilde{\mathbf{G}} \equiv \tilde{\mathbf{G}}(\mathbf{x} - \mathbf{x}', t - t')$, satisfying the relation

$$\nabla\left(\nabla\cdot\tilde{\mathbf{G}}\right) - \nabla^2\tilde{\mathbf{G}} - k_0^2\tilde{\varepsilon}\cdot\tilde{\mathbf{G}} = -4\pi\delta(\mathbf{x} - \mathbf{x}')\delta(t - t')\tilde{\mathbf{I}} \tag{4}$$

where $\tilde{\mathbf{I}}$ is the identity matrix. Now, following the standard Green's function analysis [*Jackson*, 1975], the expression for the electric field is found to be

$$\mathbf{E}(\mathbf{x},t) = -\frac{ik_0^2}{(2\pi)^4\omega_0}\int d^3k \int d\omega\, \tilde{\mathcal{G}}(\mathbf{k},\omega)\cdot \mathcal{J}_A(\mathbf{k},\omega) e^{i\mathbf{k}\cdot\mathbf{x}} e^{-i\omega t} \qquad (5)$$

with the magnetic field related via Maxwell's equations. The script variables, $\tilde{\mathcal{G}}$, and $\mathbf{J}_A$, are the Fourier transforms of the Green's function tensor and the antenna current. The integrals are evaluated numerically at the desired spatial locations.

A comparison of a typical measured antenna radiation pattern with the corresponding calculated pattern is shown in Plate 3.

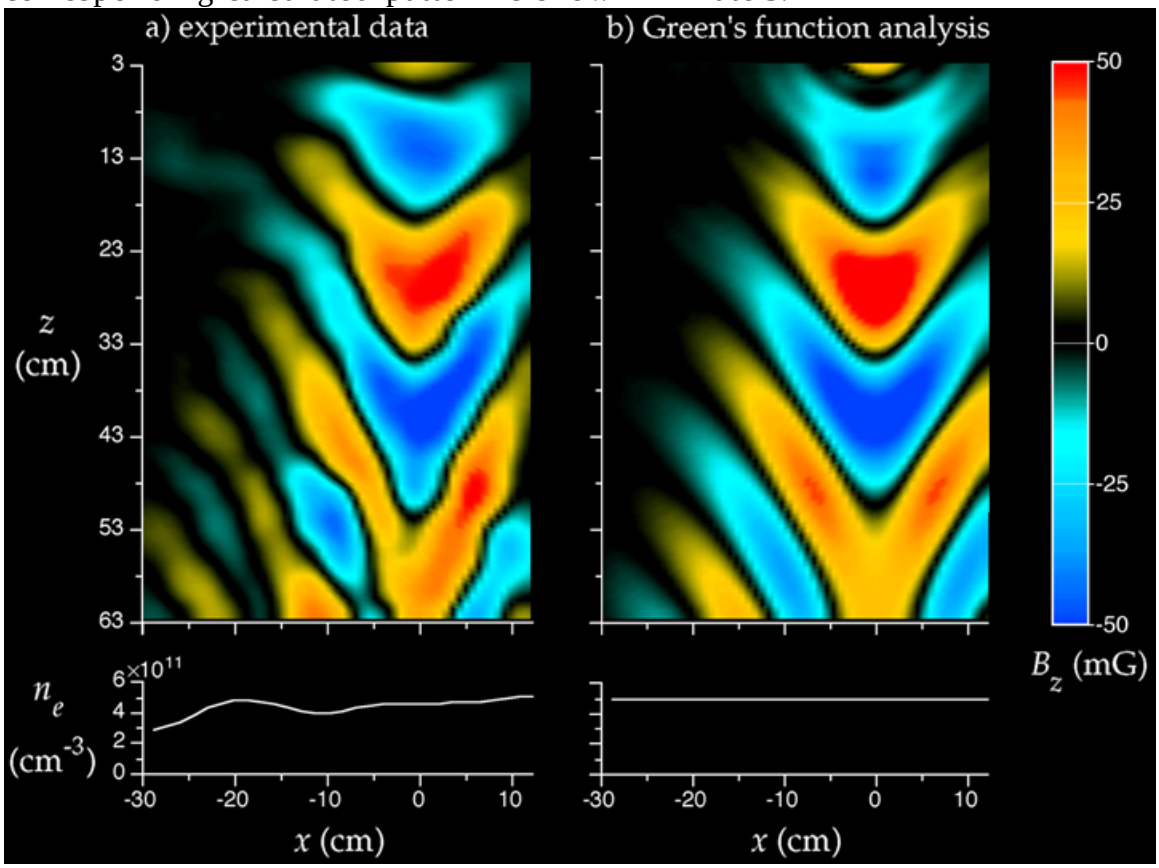


**Plate 3.** Comparison of Green's function predicted antenna radiation pattern with experimental data taken in a nearly uniform plasma. The pattern is calculated for the following experimental parameters: a magnetic field of 540 G, a frequency of 80 MHz, and a density of $5\times10^{11}$ $cm^{-3}$. The antenna is located at the origin, but 5 cm above the data planes shown here. The view is

perpendicular to the background magnetic field (the field being parallel to the $z$-axis). Wave field data is color-coded with blue representing the most negative values and red the most positive as indicated by the color bar to the right. This same representation scheme is used throughout the paper. Below each radiation pattern, the density profile is shown for reference.

The antenna is located at the origin and the data plane is defined by $-30 < x < 12.5$, $3 < z < 63$, and $y = -5$ cm. For this case, the key parameters are $f = 80$ MHz, $B_0 = 540$ G, and $n_e = 5\times10^{11}$ cm$^{-3}$. In Plate 3(a), the $B_z$ component of the measured wave magnetic field is shown. The $B_z$ values are color-coded with red indicating positive $B_z$, blue for negative $B_z$, and black for $B_z = 0$ (see the color bar on the far right). Note that this same scheme of representing 2-dimensional wave field data is used throughout the paper. Below the measured radiation pattern is the density profile. In Plate 3(b), the corresponding radiation pattern calculated using the Green's function analysis is shown. The density profile in this case is, of course, perfectly flat. The first point is that generally the data match well to the predicted pattern even though the plasma is bounded (the column diameter is 4–5 perpendicular whistler wavelengths) and not entirely uniform. Discrepancies appear only on the left hand side ($-30 < x < -10$ cm) where the density becomes non-uniform. We have made further comparisons between data and Green's function analysis output for different experimental parameters ($n_e$, $B_0$, and $f$) in cases of varying degrees of plasma homogeneity and we find equally good agreement in those regions where the plasma density is nearly uniform. It is concluded that the behavior of the whistler wave radiation of our antenna in a uniform or near-uniform plasma is well understood, agreeing with the predictions of linear, cold plasma theory. The second point to be made with

regard to the antenna radiation in a uniform plasma is that detailed analysis reveals no evidence of waves with wavelengths shorter than the whistler wavelength. Hence, we conclude that our antenna does not itself launch lower hybrid waves, nor do lower hybrid waves appear via some other mechanism in a uniform or near-uniform plasma.

## Experimental Data

In our most recent experiments, a single-frequency electromagnetic whistler wave is launched into a region of plasma containing a field-aligned density striation. The $B_z$ component of the resulting wave field pattern is measured in a horizontal ($x$-$z$) plane bisecting the striation. Details of the experimental geometry are given in Fig. 4.

(a) top view

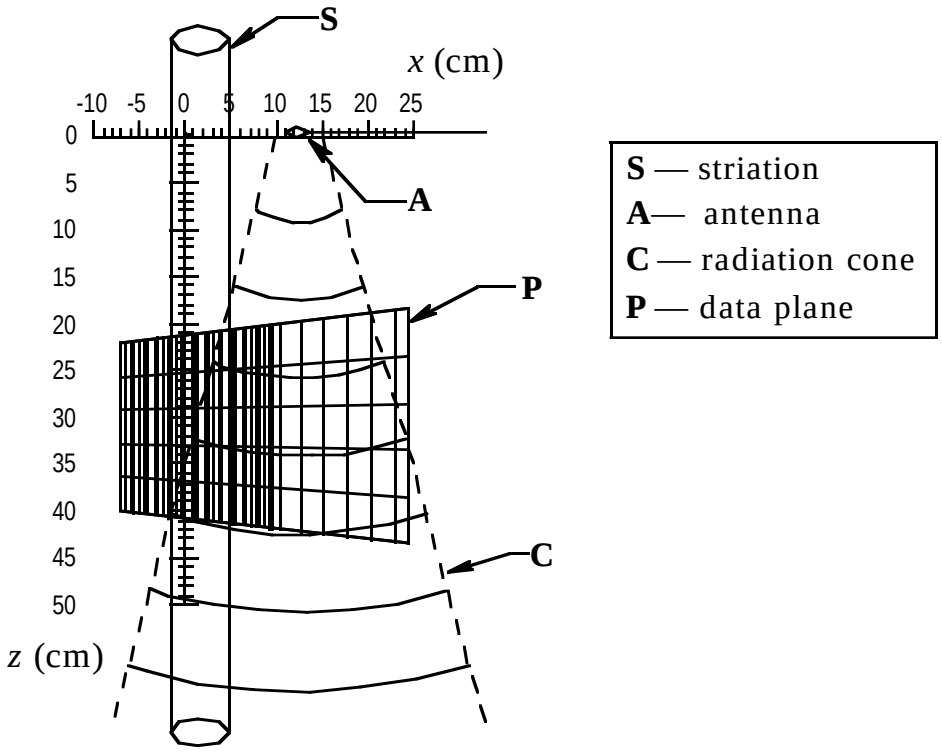


(b) axial view

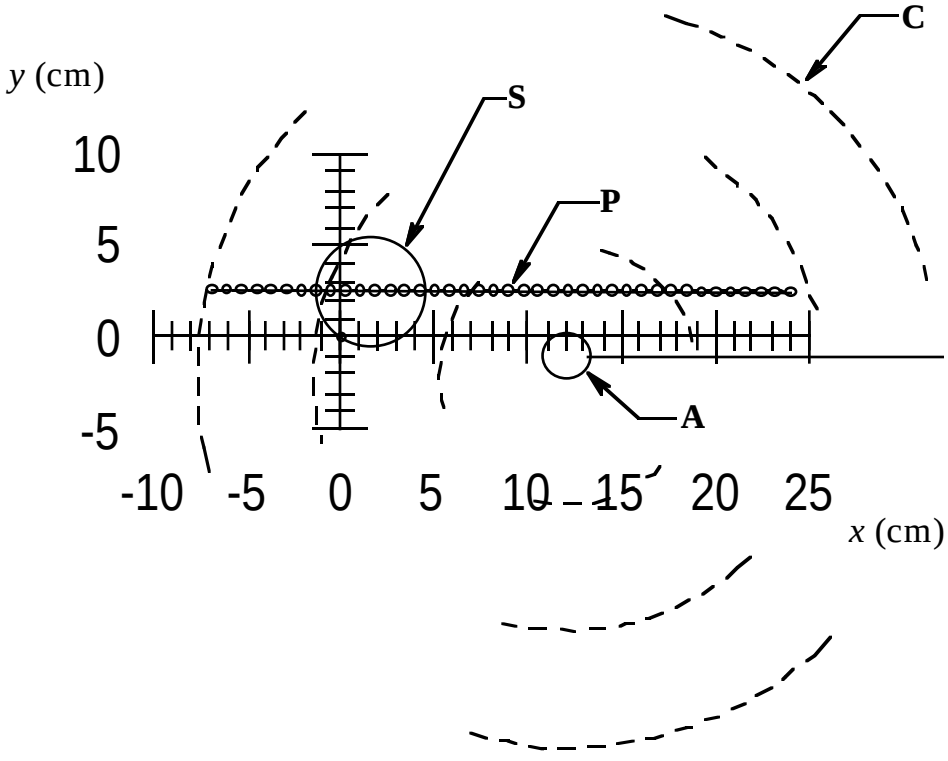


**Figure 4**

**Figure 4.** Schematic drawings of experimental setup for horizontal plane data. The perpendicular view (a) and axial view (b) show the spatial relationship between the striation (S), antenna (A), radiation cone (C), data plane (P), and coordinate axes (lines with hash marks centered at the origin). The measurement grid, in (a), shows every fourth data line.

Across the magnetic field (in the *x*-direction), measurements are made over a broad region around the striation as well as over the full width of the antenna radiation pattern. The measurement range along the magnetic field (in the *z*-direction) includes more than one full parallel whistler wavelength, centered on the region where the interaction is expected to occur. Note from Fig. 4(b) that the measurement plane is located slightly above the antenna. Data locations are more finely spaced across $\mathbf{B}_0$ in the vicinity of the striation (0.1 cm) in order to adequately resolve the mode-converted lower hybrid waves ($\lambda_{\perp,LH}$ = 1.5 cm); the plane contains a total of 3980 locations (only every fourth grid line is shown in Fig. 4).

The raw data are shown in Plate 4 as a color-coded snapshot of the wave field pattern at a single moment in time. Below this is a plot of the plasma density along a line through the center of the data plane at $z$ = 30 cm. Two important features are observed in the wave field data in Plate 4. First, just outside the striation edge, the field pattern is sharply disrupted (compare to the uniform case in Plate 3).

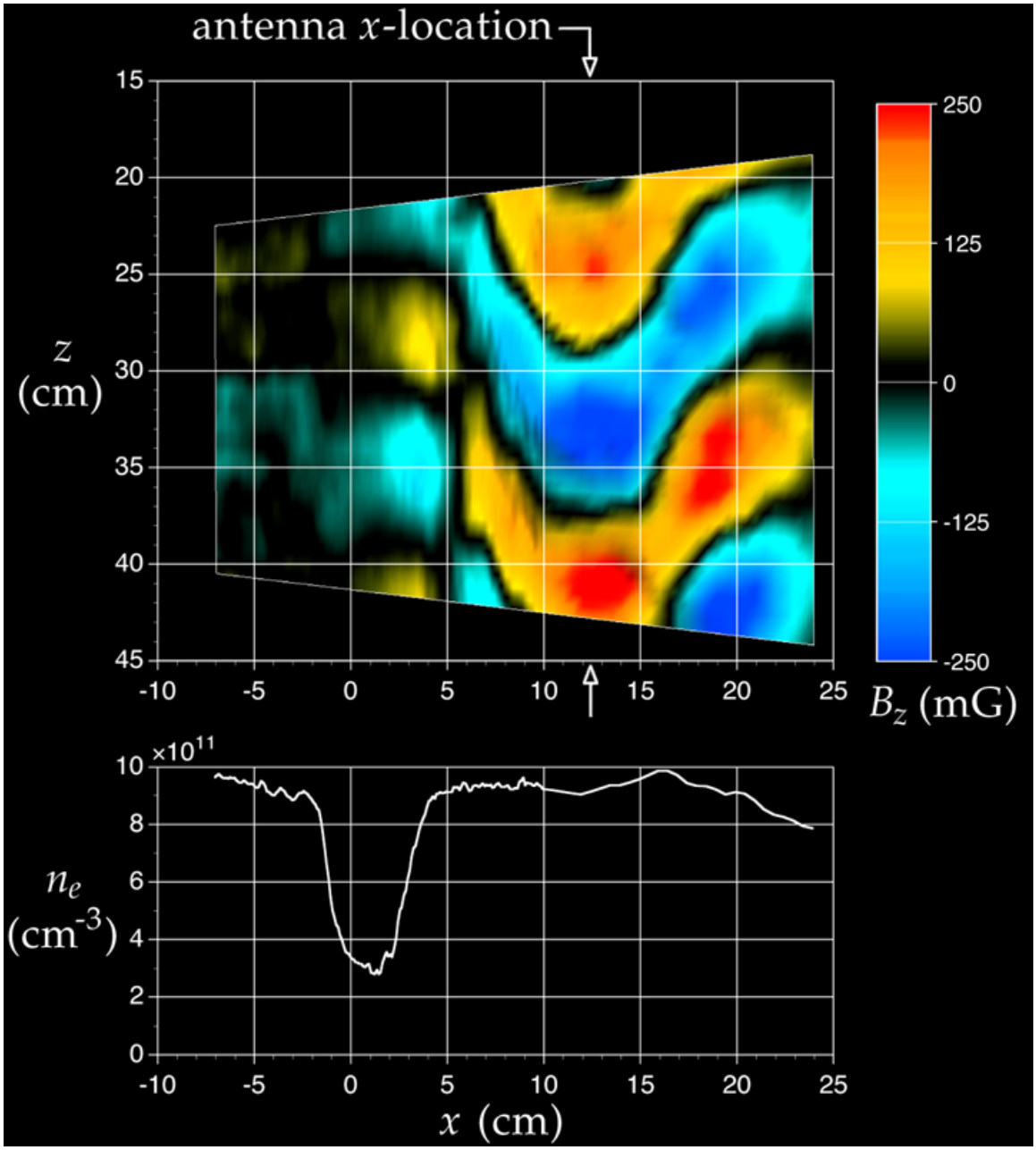


**Plate 4.** Measured $B_z$ wave field data in a 2-D ($x$, $z$) plane through the center of the density striation. The view is perpendicular to the background magnetic field. A radial profile of the plasma density is shown below for reference. The edge of the striation is at $x$ = 3.8 cm. The antenna $x$-location is indicated with arrows at $x$ = 12.2 cm.

A 180° phase shift, in the perpendicular direction, occurs at $x \approx 5$ cm, over a space of only 1 cm. This phase shift is most clear for $z > 30$ cm but also extends back to $z \approx 25$ cm. The phase shift also corresponds to a marked amplitude minimum which runs parallel to the striation edge at $x = 5.5$ cm. These characteristics indicate that superposition of the incident whistler waves with reflected whistler waves is taking place in the vicinity of the striation boundary, as discussed in more detail below. The second important feature is that the wave pattern shows evidence of short wavelength structure near the striation edge. It is most easily seen between $x = 5$ and 10 cm in the yellow colored phase front. This short wavelength structure, although only faintly seen here in the raw $B_z$ data, is revealed much more clearly in the detailed analysis below.

At this point, in order to extract more detailed information, we decompose the data into phase and amplitude components which allows the long wavelength and short wavelength effects to be separated.

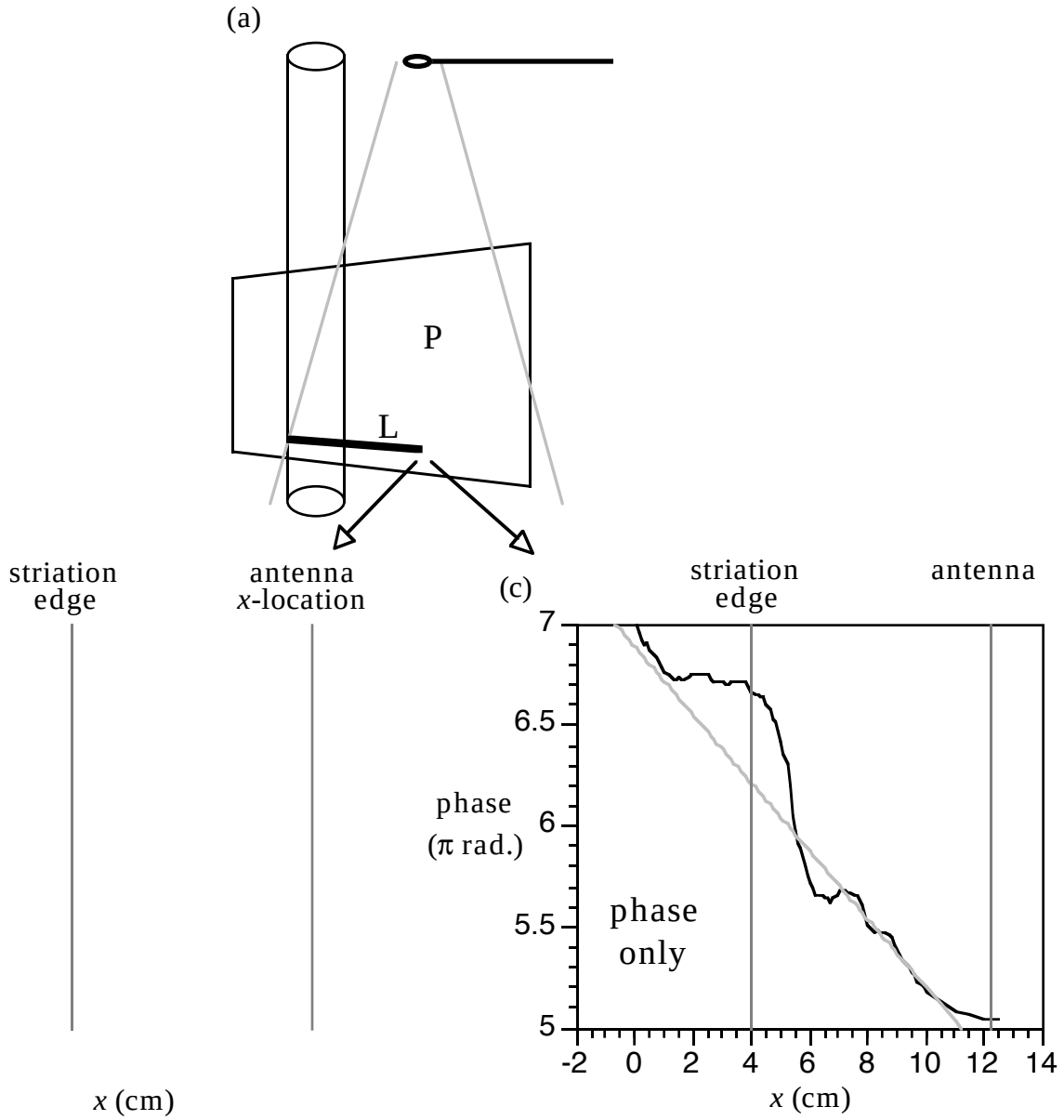


**Figure 5.** 1-D $B_z$ data separated into amplitude and phase components. A schematic diagram (a) shows the spatial relationship between the antenna, striation, data plane (P) and a linear subset of the data (L) in the interaction region. The amplitude-only data, $|B_z|$, are shown in (b) and the phase-only data in (c) which also contains a straight line fit to the data calculated for the region $7 < x < 10$ cm. The slope of this line yields the incident whistler

wavelength. Also in the plots, (b) and (c), the *x*-locations of the striation edge and the antenna are indicated by vertical lines.

The phase, in particular, turns out to be a very sensitive and useful measure of the wave properties. The decomposition is shown in Fig. 5 for a 1-D cut along *x* through the interaction region. Fig. 5(a) shows the location of the data line, L, within the data plane, P. Amplitude is plotted in Fig. 5(b) and phase in Fig. 5(c). These quantities are derived from the time series, recorded at each location, which takes the form of a sine wave. The amplitude is just the amplitude of the sine wave and the phase is relative to that of the input signal at the antenna. The two graphs, Figs. 5(b) and 5(c), taken together exhibit all five modes expected in the interaction, namely the incident and reflected whistler wave, the evanescent transmitted whistler, and the reflected and transmitted lower hybrid waves (though, in fact, these last two modes are not actually reflected or transmitted, being mode-converted at the striation boundary itself). The interpretation, however, is not entirely straightforward so we will discuss each mode in turn.

From the full horizontal plane data, Plate 4, it is clear that there are incident whistler waves. They have a fairly limited **k**-spectrum as evinced by the existence of well defined phase fronts, especially in the interaction region. Therefore, for the sake of discussion, we assume that this limited spectrum may be replaced by a single **k** at the peak of the spectrum. In Fig. 5(c), the phase increases, to the left, away from the antenna. We take the average slope of the phase between x = 7 and 10 cm as an estimate of the incident whistler wave number in the x-direction, $k^I_{x,W}$. This slope is $k^I_{x,W} = -0.53 \pm 0.10\ \mathrm{cm}^{-1}$ which corresponds to a measured wavelength, in the *x*-direction, of $\lambda^I_{x,W} = 12 \pm 2$ cm. However, since the measurement line is at an angle to the

incident **k** due to the placement of the antenna below the measurement plane (see Fig. 4), the actual incident whistler *perpendicular* wavelength is shorter. In the region where the slope of the phase is measured, this angle averages to approximately 30°. Thus, the incident whistler perpendicular wavenumber is actually $k^I_{\perp,W} = -0.61 \pm 0.12\ \mathrm{cm}^{-1}$ which corresponds to a perpendicular wavelength of $\lambda^I_{\perp,W} = 10 \pm 2$ cm.

The parallel wavenumber is found by calculating the slope of the phase vs. $z$ (not shown here). The result is $k_{\|} = 0.38 \pm 0.02\ \mathrm{cm}^{-1}$, or $\lambda_{\|} = 16.5 \pm 0.8$ cm. The estimation of $k_{\|}$ is more accurate than in the perpendicular case because the variation of the phase with $z$ is very regular. As a check, when this value of $k_{\|}$ is substituted into the dispersion relation (1), using the density, magnetic field, and wave frequency given above, one finds the predicted value for $k_{\perp,W}$ to be $-0.63\ \mathrm{cm}^{-1}$, which is well within the uncertainty range of the experimental value.

Now, if the incident whistler wave were the only wave present, as in the uniform case, the amplitude would smoothly decrease, and the phase would smoothly increase, away from the antenna. This is clearly not the case here, in Fig. 5, with the addition of the striation. The most obvious difference appears just outside the striation at $x = 5.4$ cm (1.4 cm outside the striation) where the amplitude exhibits a deep minimum and the phase undergoes a sharp increase of approximately $\pi$ radians over the space of 1.5 cm. The amplitude minimum position, at $x = 5.4$ cm, corresponds to the position of the center of the phase shift (±3 mm). The amplitude minimum position remains fixed (within ±5 mm) for changes in density, wave frequency, and magnetic field strength, as well as for changes in input signal strength and in the distance from the antenna to the striation. The coincidence of the amplitude minimum with the center of the phase shift is also unaffected by these changes. The

combination of these two features is characteristic of an anti-node in the superposition of two oppositely directed waves, as illustrated in Fig. 6, in which the amplitude and phase data have been replotted as points. Superimposed are the resultant amplitude and phase of the sum of two oppositely directed plane waves (opposite in the *x*-direction).

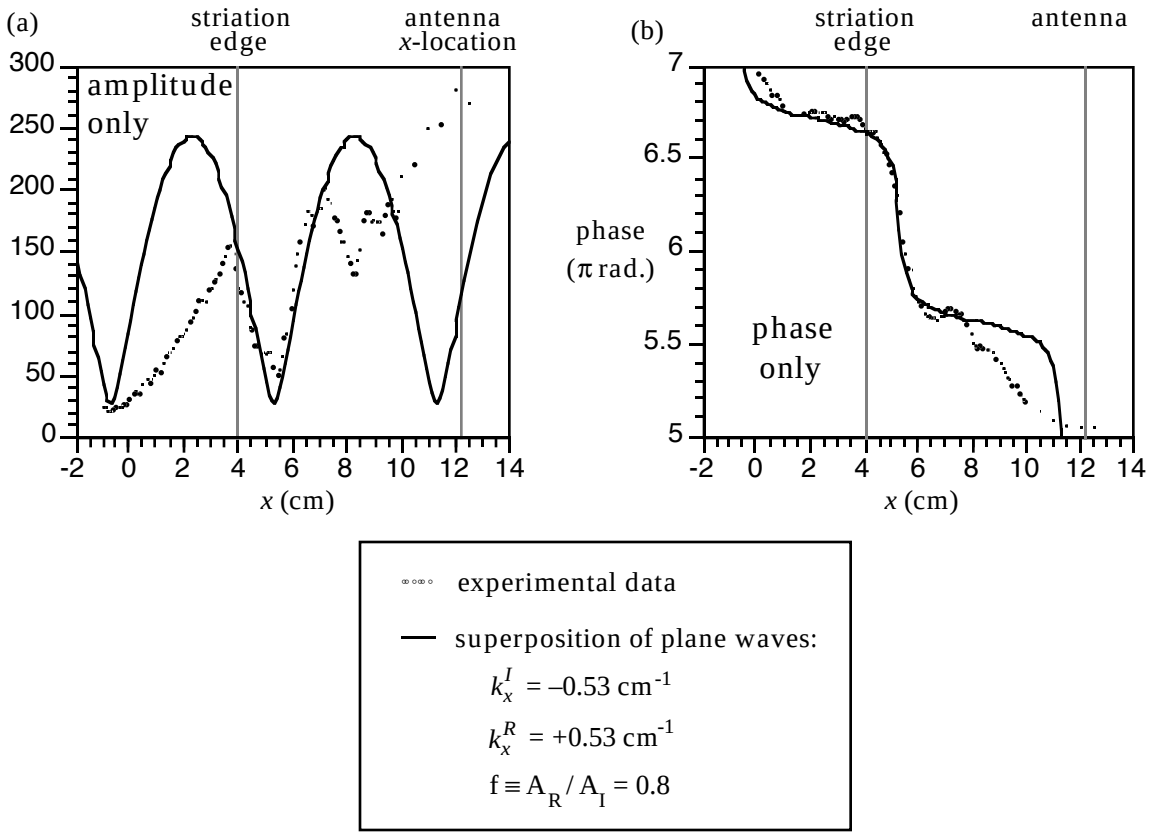


**Figure 6.** Comparison of experimental data with the superposition of two oppositely directed plane waves. The data are decomposed into amplitude (a) and phase (b) components for the same linear subset as in Fig. 5. The plane waves are meant to represent the incident and reflected whistler waves. Wave numbers and relative amplitudes of the two plane waves are adjusted to give the best fit in the region $4 < x < 8$ cm. The result is wave numbers of

$k_x^I = -0.53\ \text{cm}^{-1}$ and $k_x^R = +0.53\ \text{cm}^{-1}$ for the incident and reflected plane waves, respectively, and a relative amplitude of 0.8 of the reflected wave. When corrected for the angle between the data line and the perpendicular direction for the waves, the wave numbers fall on the wave normal curve to within 1% (see Fig. 8).

The expression used is:

$$A(x)e^{i\Phi(x)} = S\left[e^{ik_x^I x} + fe^{i\left(k_x^R x + \phi_0\right)}\right] \tag{6}$$

where $A$ and $\Phi$ are the resultant amplitude and phase, now both functions of $x$. The important quantities on the right hand side of the equation are $k_x^I$, the wave number of the left-going wave of the superposition (representing the incident wave); $k_x^R$, the wave number of the right-going wave (representing the reflected wave); and $f$, the fractional amplitude of the right-going wave. As for the other two parameters, $S$ is used for overall amplitude scaling and $\phi_0$ is used to shift the pattern in $x$. The value of $k_x^I$ is chosen to be the apparent value of $-0.53\ \text{cm}^{-1}$ (this value, as opposed to the corrected value, is used because we are trying to match to the actual data which are taken on a line angled with respect to the perpendicular direction). The best correspondence to the data, shown in Fig. 6, is found for $k_x^R = +0.53\ \text{cm}^{-1}$ and $f = 0.8$;. That is, the reflected wave having $k_x$ equal and opposite to the incident and having an amplitude 80% of the incident (the absolute incident whistler wave amplitude, in the vicinity of the striation, is estimated to be 140 mG). The fit is still reasonable for $k_x^R$ varying by $\pm 0.10\ \text{cm}^{-1}$ and $f$ varying by $\pm 0.1$.

In the amplitude data of Fig. 6(a), the experimental curve matches the two-wave superposition in the region between $x = 4$ and 7 cm, centered on the

amplitude minimum. This fact, combined with the coincidence of the sharp phase shift at x = 5.4 cm in Fig. 6(b), confirms the existence of a reflected whistler wave in this region. Note that if we assume the angle of reflection equals the angle of incidence (which is reasonable since the data plane is taken at the midline of the striation), then the actual reflected whistler perpendicular wave number, after correction, is $k_{\perp,W}^{R} = +0.61 \pm 0.10\ \mathrm{cm}^{-1}$.

It can be seen, in Fig. 6(b), that the superposition phase corresponds closely to the data over the range $-1.0 < x < 7.5$. Only the region from x = 3.7 to 7.5 cm, outside the striation, corresponds to the reflected whistler wave. The part of this range which lies inside the striation, $-1.0 < x < 3.7$, contains the evanescent transmitted whistler wave. This is seen most clearly in the amplitude data which abruptly changes slope at $x = 3.7$ cm, just inside the striation boundary, and drops off exponentially as one moves into the striation. Combined with this, the phase is seen to be nearly flat (the slight slope is accounted for by the fact that the data are taken along a line which has a small component along $z$). The combination of exponential decay in the amplitude and unchanging phase are features of an evanescent wave. Recall from the discussion of Fig. 3 that the low density within the striation is unable to support a propagating whistler mode, given the parallel wavelength of the launched wave. An exponential fit to the section of data inside the striation yields a $k_\perp$ value of $k_{\perp,W}^{T} = 0.45i \pm 0.02i$; the value predicted by the cold plasma dispersion relation (1), using the minimum density in the striation, is $0.36i$. That is, the decay is calculated to occur over a slightly longer distance. The difference is attributable to the additional amplitude provided by the transmitted lower hybrid wave near the striation boundary which makes the decay appear to be more rapid. (The presence of these lower hybrid waves is established below.) The sharpness of the change in the amplitude profile at

$x$ = 3.7 cm is interesting because it indicates that reflection may occur over a shorter distance, a few mm, than the density gradient scale length, ~1.5 cm.

Now that the long wavelength features of the interaction have been identified, we turn to the problem of extracting evidence for the mode-converted lower hybrid waves. The main difficulty lies in the fact that a much smaller portion of the wave energy density goes into the magnetic field of these waves as compared to the whistler waves. The energy density in a plasma [*Stix*, 1962] is

$$U = \frac{1}{16\pi}\left[\mathbf{B}^{*}\cdot\mathbf{B} + \mathbf{E}^{*}\cdot\frac{\partial}{\partial\omega}\left(\omega\tilde{\varepsilon}\right)\cdot\mathbf{E}\right]. \qquad (7)$$

In Fig. 7 we plot the ratio of the wave energy density contained in the (measured) $B_z$ component to the total wave energy density (*i. e.* $\frac{1}{16\pi}B_z^2/U$), as a function of $k_\perp$.

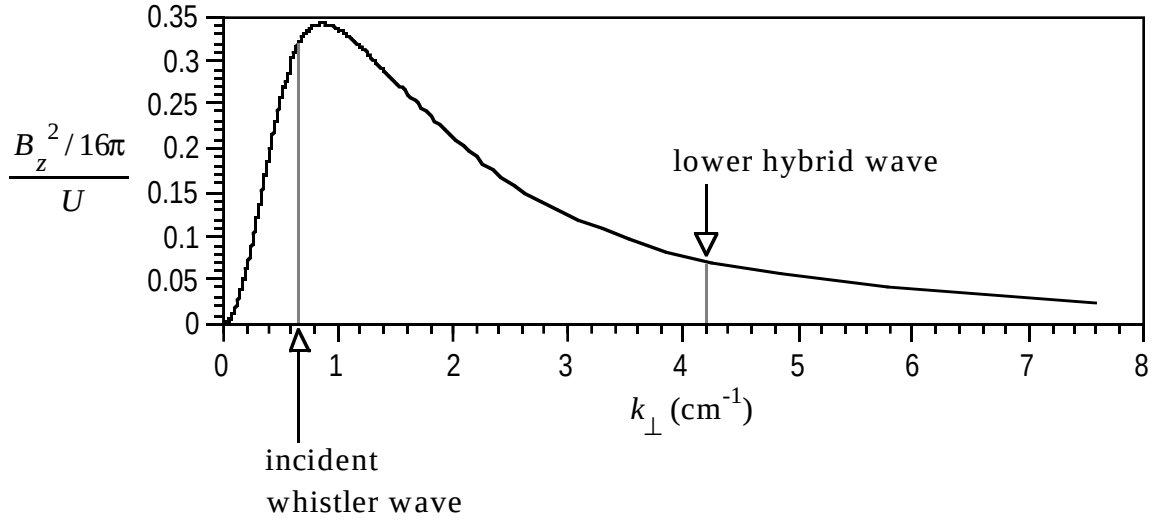


**Figure 7.** Fraction of wave energy density contained in the wave $B_z$ component as a function of $k_\perp$. The fraction of the wave energy density peaks at a $k_\perp$ value near that of the incident whistler wave. At typical lower hybrid wave $k_\perp$ values, the fraction is about 5 times lower.

The $k_\perp$ of the incident (and reflected) whistler waves and the expected $k_\perp$ of the lower hybrid waves are both highlighted. The dividing line between the two modes, as discussed in conjunction with Fig. 3, is at $k_\perp \approx 1.8\ \mathrm{cm}^{-1}$. It can be seen that lower hybrid waves, sometimes referred to as "electrostatic whistlers", in fact have a small magnetic field component. In our case, the fraction of the wave energy that goes into the $B_z$ component in the case of the lower hybrid waves is about 5 times smaller than in the whistler case. This means that even if the energy density of the two waves were equal, a $B_z$ probe would measure the whistler wave amplitude to be 5 times larger than the lower hybrid wave amplitude. Thus, one expects that the lower hybrid waves will appear as short wavelength, low amplitude perturbations on the overall long wavelength pattern. The phase-only representation is very useful in revealing these perturbations. For example, in Fig. 6(b), between $x = 1$ and 4 cm, two short wavelength oscillations can be seen. Also, between $x = 6$ and 9 cm, another two short wavelength oscillations are visible. These are due to lower hybrid waves; transmitted lower hybrid waves inside the striation, reflected lower hybrid waves outside. Similar perturbations are seen on each data line for z > 30 cm.

At this point, it is worth considering the details of the situation. The long wavelength whistler components taken together may be represented as $A_1(x)e^{i\varphi_1(x)}$. Either one of the lower hybrid waves may be individually represented as $A_2(x)e^{ik_2x}$, assuming that its perpendicular wave number spectrum is peaked at $k_2$. Now, we write the sum of the two above expressions as:

$$M(x)e^{i\theta(x)} = A_1(x)e^{i\varphi_1(x)} + A_2(x)e^{ik_2x} \qquad (8)$$

with the goal of finding $M(x)$ and $\theta(x)$. If, for a given $x$, the amplitude of the lower hybrid wave is smaller than the overall amplitude of the long wavelength waves, then it is straightforward to show that

$$M \approx A_1[1+\varepsilon\cos(\varphi_1 - k_2 x)] \tag{9}$$

$$\theta \approx \varphi_1 + \varepsilon\sin(k_2 x - \varphi_1)\,, \tag{10}$$

which relations hold as long as the condition

$$\varepsilon \equiv A_2/A_1 \lesssim 0.5 \tag{11}$$

is satisfied. Now, from equations (9) and (10), it can be understood why it is easier to see the perturbations in the phase as opposed to the amplitude. The perturbations in equation (9) are not only added on to $A_1$ (which, in our case, is a steeply sloped function of $x$), but are also multiplied by it. This makes the perturbations quite difficult to see. On the other hand, in equation (10) the phase perturbations are only added to $\varphi_1$. The function $\varphi_1$, as we have seen, is slowly varying except for limited regions in $x$; that is to say, normally $d\varphi_1/dx << k_2$. The result is nearly sinusoidal oscillations superimposed onto the slowly varying background phase. These oscillations have an apparent wave number of approximately $k_2$ and an amplitude, $\varepsilon$, equal to the ratio of the lower hybrid wave amplitude to the background amplitude as a function of $x$. Thus, by measuring the spacing between perturbation peaks in the data, the lower hybrid wavelength may be estimated. Furthermore, by measuring the offset of the peaks from the background phase (in radians), and multiplying this by the background amplitude, the lower hybrid wave amplitude may be estimated.

Applying this technique to Fig. 6(b), we find that, for this particular data line, the transmitted lower hybrid wave has a wavelength of $\lambda_{\perp,LH}^{T}$ = 1.4±0.1 cm and an amplitude of 3.5±0.5 mG near the striation edge. The reflected lower hybrid wave, for this case, has a wavelength of $\lambda_{\perp,LH}^{R}$ = 1.3±0.1 cm and an amplitude of 27±2 mG at x = 7 cm. Note that these wavelengths are somewhat shorter than the typical values discussed below. The amplitudes are 2% and 15%, respectively, of the local total wave amplitude which turn out to be very close to the typical values. The comparison in terms of wave energy density is discussed below. However, at this point, we extend this technique by applying it to all the data lines using the following procedure. The locations of all visible short wavelength peaks and troughs are recorded. For any one peak, the deviation (in radians) from the overall phase curve is estimated by taking half of the difference between the peak and a straight line drawn between the adjacent troughs. Separations between the peaks must also be corrected for the slope of the background phase $\varphi_1$. Trough deviations and separations are estimated in an analogous way. The information gained, namely the locations and sizes of the lower hybrid wave peaks and troughs, is then used, in effect, to filter out the long wavelength data, leaving an approximation of the lower hybrid wave pattern as a function of $x$ and $z$. The procedure fails in the region $4.7 < x < 5.7$ cm where the background amplitude is too small to satisfy condition (11) and the phase changes too rapidly to make a good estimate of the peak (or trough) location and amplitude. In this region, we interpolate between the regions on either side.

The result of the procedure just described is shown in Plate 5.

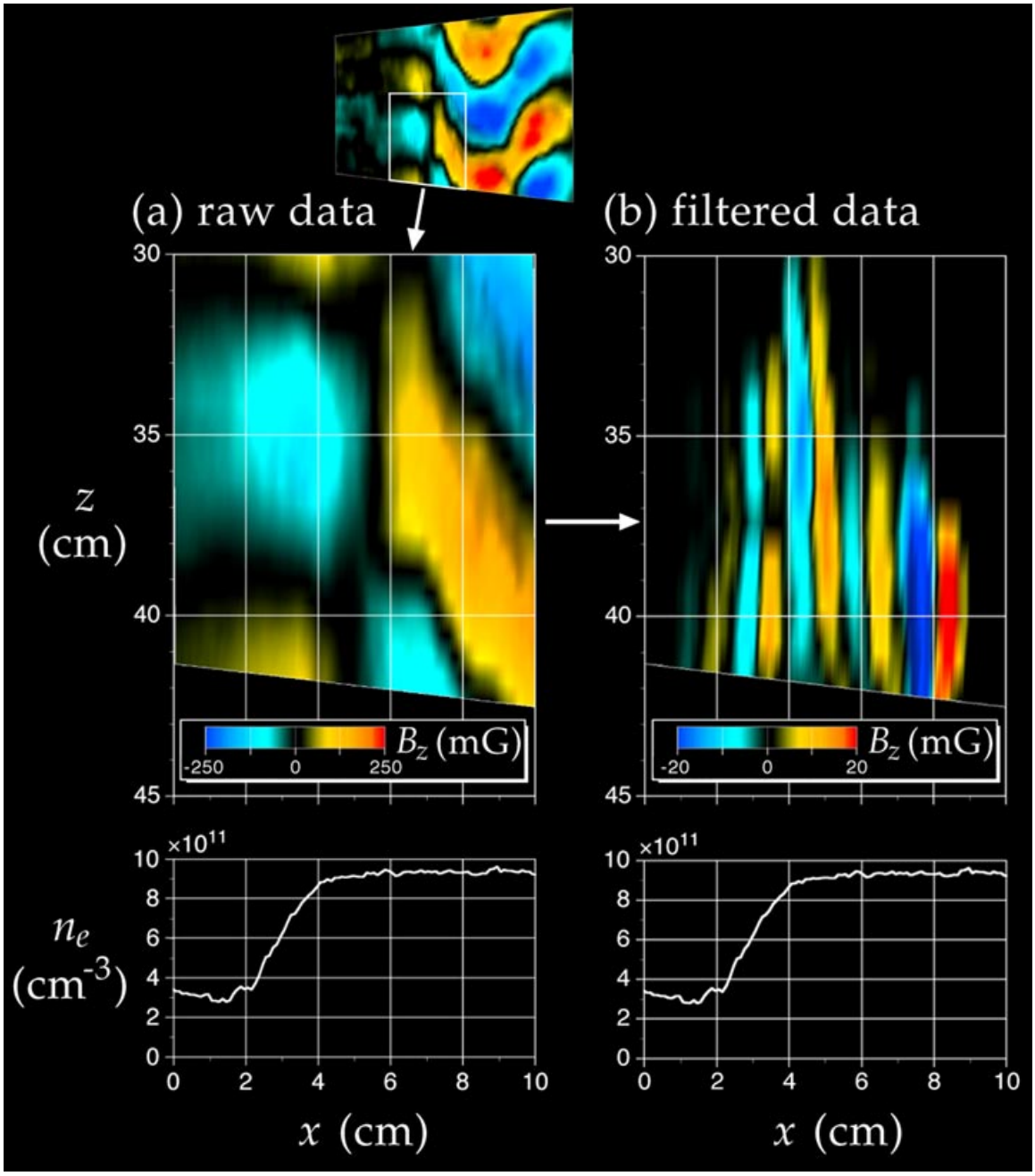


**Plate 5.** Detailed view of measured $B_z$ wave field data in the interaction region. Data are shown raw in (a) and with long wavelengths filtered out in (b). The filtering process is described in detail in the text. As in Plate 4, the view is perpendicular to the background magnetic field and radial profiles of the plasma density are given below for reference. When the long wavelength,

higher amplitude whistler waves are removed, lower hybrid waves can be clearly seen.

The raw data in the interaction region are magnified in Plate 5(a) and the filtered data in this region are shown in Plate 5(b). Several important observations may be made here. First, the peak and trough data, when combined in this fashion, clearly resolve themselves into phase fronts which have the properties expected for lower hybrid waves. The phase fronts are nearly, but not exactly, aligned with the *z*-axis. A close examination reveals that, on either side of the striation boundary, at $x = 4$ cm, the phase fronts are angled such that their corresponding wave vectors point toward the boundary with a very small component pointing along $\hat{\mathbf{z}}$. (We know the wave vectors are not pointing away from the boundary because that would imply $k_{||}$ in the negative *z*-direction.) Thus, the reflected and transmitted lower hybrid waves propagate towards each other. This is just what is expected for the lower hybrid wave which, in the perpendicular direction, is a "backwards propagating" wave. (Lower hybrid waves with this backward-propagation property, launched with an antenna as opposed to mode-converted from a striation, were first observed in a laboratory plasma by *Stenzel and Gekelman* [1975].) The energy of these waves, on the other hand, radiates primarily along *z* with a small component away from the boundary.

From a detailed analysis of the peak and trough data underlying Plate 5, we calculate typical perpendicular and parallel wavenumbers, as well as typical and maximum wave amplitudes for both the reflected and the transmitted lower hybrid waves. The results are summarized here. The transmitted lower hybrid waves, to the left of $x = 3.8$ cm, have a perpendicular wavelength of $\lambda_{\perp,LH}^{T} = 1.46 \pm 0.15$ cm or, equivalently, $k_{\perp,LH}^{T} = +4.3 \pm 0.4$ cm$^{-1}$.

On the other side of the striation, the reflected lower hybrid waves exhibit a perpendicular wavelength of $\lambda^R_{\perp,LH} = 1.50\pm0.07$ cm and a corresponding wavenumber of $k^R_{\perp,LH} = -4.2\pm0.2$ cm$^{-1}$. Parallel wavenumbers for the lower hybrid waves are much more difficult to estimate because their angle with respect to z is so shallow (< 5°). We find for the transmitted waves, $\lambda_{\parallel} = 21.1\pm11.9$ cm, and for the reflected waves, $\lambda_{\parallel} = 35.6\pm21.5$ cm. These are both larger than the value of 16.5 cm calculated above, but the error ranges are large enough to include it.

All of the observed wave numbers are conveniently summarized using the wave normal curves as shown in Fig. 8.

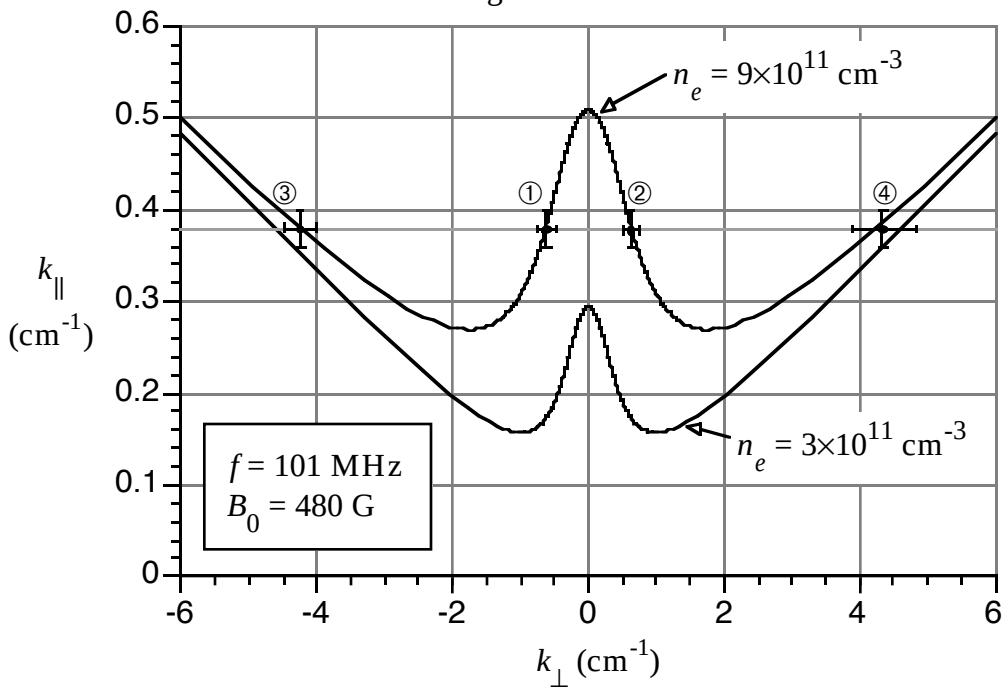


| | | |
|---|---|---|
| ① | incident whistler | $k^I_{\perp,W} = -0.61 \pm 0.12$ cm$^{-1}$ |
| ② | reflected whistler | $k^R_{\perp,W} = +0.61 \pm 0.10$ cm$^{-1}$ |
| ③ | reflected lower hybrid | $k^R_{\perp,LH} = -4.2 \pm 0.2$ cm$^{-1}$ |
| ④ | transmitted lower hybrid | $k^T_{\perp,LH} = +4.3 \pm 0.4$ cm$^{-1}$ |

**Figure 8.** Measured ($k_\perp$, $k_\parallel$) values for the four propagating modes are plotted over the wave normal curves corresponding to the plasma density outside the striation and the minimum density inside the striation. The common $k_\parallel$ value is indicated by the dotted line at 0.38 $cm^{-1}$. Modes ① to ③, the whistler modes and the reflected lower hybrid mode, lie, as expected, on the high density curve (to within 1%). Mode ④, the transmitted lower hybrid wave, lies between the high and low density curves. What value the transmitted lower hybrid wave $k_\perp$ should have is not clear, but it must be somewhere between the two curves.

The upper curve is calculated for the density outside the striation, $9\times10^{11}$ $cm^{-3}$, and the lower curve is for the minimum density within the striation, $3\times10^{11}$ $cm^{-3}$, as in Fig. 3. The combined ($k_\perp$, $k_\parallel$) of the four observed wave modes are plotted as points labeled ① through ④. Modes ① to ③, the whistler waves and the reflected lower hybrid wave, propagate outside the striation in the high density region. As such, they are expected to lie on the upper curve which, in fact, they do with great accuracy. The difference between the predicted and observed values is less than 1%, well within the experimental error of, typically, ±5% for these modes. Mode ④, the transmitted lower hybrid wave, propagates inside the striation boundary where the density changes over a very short distance. Its $k_\perp$ is expected to lie somewhere between the high and low density curves, 4.5 $cm^{-1}$ for example, which corresponds to a density half way between the two extremes. The observed value is much closer to the high density curve at 4.3 $cm^{-1}$; however, the error associated with its measurement is large enough to include the entire range between the two curves.

We now focus attention on the observed amplitudes of the lower hybrid waves. For the transmitted lower hybrid waves, the typical amplitude is 3.6±1.7 mG, which is 3% of the background wave amplitude. Spatially, the amplitude tends to be highest near the striation edge and to drop off as one moves into the striation. After about 2 perpendicular wavelengths, transmitted lower hybrid waves can no longer be observed. The reflected lower hybrid wave amplitude, on the other hand, behaves somewhat differently. It drops as one moves away from the edge for ~2 $\lambda_{\perp,LH}$, then increases to a much higher amplitude for another $\lambda_{\perp,LH}$, after which it drops to zero. The appearance of lower hybrid waves so far from the striation boundary is contrary to the sharp planar interface model. Waves generated at the interface in this model are expected to radiate at the group velocity angle appropriate to the mode in question. For the lower hybrid waves, this angle is 3.5°. Thus, at $z$ = 42 cm, ~12 cm from the start of the interaction region, lower hybrid waves are expected to exist only 0.7 cm (half a perpendicular wavelength) from the striation boundary. In fact, they are seen 2-3 perpendicular wavelengths away. The experimental situation differs from the model in two ways: 1) the striation is cylindrical and 2) the interface is not sharp — the gradient scale length is on the order of the lower hybrid perpendicular wavelength. We speculate that the second dissimilarity is more important in accounting for the existence of the mode-converted waves so far from the striation.

The typical amplitude in the region just outside the striation ($4 < x < 7$ cm) is 6.5±2.0 mG, ~5% of the incident whistler amplitude. Outside of this, in the higher amplitude region, the typical amplitude increases to 21.3±9.7 mG, ~15% of the incident whistler wave amplitude. However, the peak amplitude

in this region is 36.5 mG, which is approximately 26% of the incident amplitude.

It is worthwhile to make the above comparisons in terms of wave energy density. In order to do this, one multiplies the ratio of the squares of the observed amplitudes by the ratio of the energy density fractions, from Fig. 7, as follows:

$$u_{LH} \equiv \frac{U_{LH}}{U_W} = \frac{b_W}{b_{LH}} \frac{B_{z,LH}^2}{B_{z,W}^2} \tag{12}$$

where $b \equiv \frac{1}{16\pi} B_z^2 / U$ is the energy density fraction of either the whistler or the lower hybrid wave. Reading from Fig. 7, the values are $b_W = 0.32$ and $b_{LH} = 0.07$. Thus, for the transmitted lower hybrid wave the typical energy density, $u_{LH}^T$, is a mere 0.4% of the incident whistler wave energy density. The reflected lower hybrid wave, on the other hand, has a typical energy density $u_{LH}^R = 10\%$ of the incident. Its maximum energy density is as high as $u_{LH}^R = 31\%$ of the incident.

It is also possible to recast the comparisons in terms of the perpendicular electric field component using the polarization relations. Specifically,

$$e_{x,LH} \equiv \frac{E_{x,LH}}{E_{x,W}} = \frac{P_W}{P_{LH}} \frac{B_{z,LH}}{B_{z,W}} \tag{13}$$

where the polarization is given by *Helliwell* [1965]:

$$P \equiv \frac{B_z}{E_x} = \frac{-i\varepsilon_{xy} n \sin\theta}{\varepsilon_\perp - n^2} \tag{14}$$

and the subscripts $W$ and $LH$ imply that the values of $n$ and $\theta$ are appropriate to the whistler and the lower hybrid mode, respectively. For our conditions, $P_W / P_{LH} = 4.7$. Thus, the relative perpendicular electric field amplitudes are: typical transmitted lower hybrid wave, $e^T_{x,LH} = 14\%$; typical reflected lower hybrid wave, $e^R_{x,LH} = 71\%$; maximum reflected lower hybrid wave, $\max(e^R_{x,LH}) = 122\%$. In absolute terms, the typical value corresponds to a value of 2-3 V/cm for the reflected lower hybrid wave. All of the above comparisons are summarized in Table 2. Note that the energy densities of the mode-converted waves, since they are calculated locally, can not be used to check the energy balance with the incident wave and thus are not expected to sum to 100%. To check the energy balance one would have to integrate the energy densities over the full plasma volume.

TABLE 2. Amplitudes and energy densities of observed wave modes relative to incident whistler wave.

| wave mode | $B_z$ amplitude | energy density | $E_x$ amplitude |
|---|---|---|---|
| ① incident whistler | 100% | 100% | 100% |
| ② reflected whistler | 80% | 64% | 80% |
| ③ reflected LH (typ.) | 15% | 10% | 71% |
| (max.) | 26% | 31% | 122% |

| | | | |
|---|---|---|---|
| ④ transmitted LH | 3% | 0.4% | 14% |

## Comparison with ionospheric situation

The work presented here may be compared to the results of some experiments done in the ionosphere; in particular, those experiments in which whistler waves have been launched from the ground into striated regions of the ionosphere [*Bell et al.*, 1983; *James and Bell*, 1987; *Bell and Ngo*, 1988, 1990]. Recall that these experiments involve making electric field measurements with satellites in the low altitude (600-3800 km) ionosphere above the transmitters. During conditions where the lower hybrid resonance noise shows an irregular lower cutoff frequency, the authors find that the, originally 1 Hz bandwidth signals undergo considerable spectral broadening (up to 2 kHz). The irregular lower cutoff frequency implies that the spacecraft is passing through a region of space containing density striations. The spectral broadening, as well as several other characteristic features, implies the presence of Doppler-shifted lower hybrid waves with the same frequency as the incident electromagnetic whistler waves. That is, whistler waves are seen to mode-convert to lower hybrid waves in the presence of density striations. Bell et al. go on to propose that the mode-conversion takes place via the linear mode-coupling process at the striation boundaries; however, they are not able to observe this *directly* because the spacecraft velocity is too high.

In our experiment we do directly observe whistler wave mode-conversion to lower hybrid waves at a striation boundary in accordance with the linear mode-coupling model. We also derive from our measurements the relative amplitude of the perpendicular electric field component of the mode-

converted (reflected) lower hybrid wave with respect to the incident whistler. Its value is typically 70% and is as high as 120%, depending on the location of the observation. Typical spectrograms from the experiments in the topside ionosphere show that the reflected lower hybrid wave $E_x$ amplitude is typically approximately equal to the incident wave amplitude, ranging up to just over twice the incident amplitude [*Bell et al.*, 1983]. Thus, the typical values of both the laboratory and ionospheric experiments compare very favorably. Our experimental conditions scale reasonably well with the typical ionospheric conditions (see Table 1). Therefore, it seems certain that in the ionosphere, whistler waves do mode-convert to lower hybrid waves at the density striations via the linear mode-coupling model assumed throughout this paper. Thus, the lower hybrid waves observed are not generated by an instability associated with the density striations, but are dependent upon an external flux of incident whistler wave energy. This, we would like to stress, is our main result.

One of the motivations for investigating mode-conversion to lower hybrid waves is that LH waves are believed to be involved in the transverse acceleration of ions [*Kintner et al.*, 1992; *Vago et al.*, 1992; *Chang*, 1993]. Therefore, in order to extend our work, it is interesting to ask the question whether linear mode-conversion plays any role in generating lower hybrid waves involved in ion heating. As a first step towards answering the question, consider recent, high-resolution measurements made by rocket [*Kintner et al.*, 1992; *Vago et al.*, 1992; *Garbe et al.*, 1992]. These show very narrow density striations (~10 m across) with density depletions on the order of tens of percent. Associated with the striations are elevated $E_x$ amplitudes, typically 50 mV/m [*Kintner et al.*, 1992]. The frequencies and wavelengths associated with these wave fields lead the authors to conclude that they result from

lower hybrid waves. The elevated lower hybrid wave fields are observed on the inside of the density striations; though, in some cases they are also seen outside the striation. In association with the lower hybrid wave electric field, ions are strongly accelerated in the perpendicular direction (3 eV perpendicular temperature, up from 0.4 eV normally) [*Garbe et al.*, 1992]. In the papers quoted, the authors propose that lower hybrid collapse is responsible for their observations. However, recent calculations [*Singh*, 1994] show that the data are inconsistent in some respects with lower hybrid collapse. For the electric field strengths quoted, the density depletion should be on the order of *tenths* of a percent (as opposed to tens). Also, lower hybrid collapse cannot explain why elevated electric fields are sometimes observed outside the density striations. So it seems that lower hybrid collapse cannot entirely explain the observations. An obvious alternative source of lower hybrid (*i. e.* electrostatic whistler) waves is from electrostatic noise produced by the auroral electron beam [*Maggs*, 1989]. However, these waves are not expected to become concentrated at density striations to the extent observed. It should be noted that, unlike electromagnetic whistler waves, these auroral beam generated whistlers can not undergo linear mode-conversion at density striations because they are already electrostatic. Ray tracing analysis shows that the electrostatic whistler waves simply pass through density depletions, refracting slightly at the boundaries.

The concentration of lower hybrid waves near density striations in the ionosphere is, on the other hand, explained nicely by the linear mode-coupling model as long as a flux of electromagnetic whistlers is present; although, one caveat must be noticed with respect to our experiment. In our data, the largest fields are found outside the striation with only very small fields observed inside. This contrasts with the observation, in the ionosphere,

of the largest electric fields being inside the striation. However, there is no reason that linear mode-coupling could not produce larger amplitude fields inside the striation for different plasma parameters.

It remains to be seen how large the electric fields produced by the linear mode-conversion mechanism would be in the ionosphere, in comparison with the observed fields. To make an estimate of these based on our data, we must begin with the amplitude of the $B_z$ component of the assumed incident electromagnetic whistler wave. Unfortunately, no wave magnetic field measurements are reported in conjunction with the rocket data; however, wave magnetic field measurements have been made by *Shawhan and Gurnett* [1968] in similar regions of the ionosphere. Their data show that it is reasonable to take the incident whistler wave field $B_z$ amplitude to be 20 mγ ($2\times10^{-4}$ mG). With a conversion efficiency similar to that observed in our experiments, the mode-converted lower hybrid wave $B_z$ amplitude should be on the order of 20% of the incident, or $4\times10^{-5}$. The corresponding lower hybrid wave $E_x$ amplitude is found using the polarization relations, with the ionospheric plasma parameters and the estimated $k_x$ of the lower hybrid waves. The resulting amplitude is ~3 mV/m. This value is more than an order of magnitude smaller than the typical values reported by Vago et al. Thus, it seems unlikely that the mode-conversion mechanism studied in our experiments can account for the observed electric field amplitudes near striations in the ionosphere. However, the coupling between the whistler wave and the lower hybrid wave may be more efficient in the ionosphere than under our experimental conditions. For instance, a higher efficiency could result from the striation density gradient scale length, $L_\nabla$, being smaller in the ionosphere relative to the incident wavelength (as is generally the case). Moreover, there are situations in which absolute calibration of electric field

probes is difficult. Certainly, this is the case in the lab and there are examples where this is also the case in space (see *James* [1978]). The work of James was performed under conditions similar to that of Vago et al. and, thus, we suggest that some of the discrepancy between our projected electric field values and those quoted by Vago et al. may result from this type of calibration difficulty. In any case, from our standpoint we believe this discussion could be resolved with the addition of wave magnetic field measurements made near striations in the ionosphere. In the absence of these we can not definitively answer the question whether linear mode-conversion plays an important role in the production of lower hybrid waves involved in ion heating; however, this mechanism can not be eliminated as a possibility.

## Conclusion

In this experiment we have created a well-defined, field-aligned density striation, launched electromagnetic whistler waves which then impinge upon the striation boundary, and measured with high spatial resolution the resulting wave pattern in the interaction region. Experimental parameters are chosen such that characteristic scale length and frequency ratios closely reproduce situations found in the auroral ionosphere. We observe that the interaction of the incident whistler with the sharp density gradient at the boundary of the striation results in a reflected whistler outside and an evanescent transmitted whistler inside the striation, as well as lower hybrid (or "quasi-electrostatic whistler") waves both inside and outside the striation. The observed perpendicular wavenumbers of all the modes agree very well with the predictions of the linear mode-coupling model (within ±1%). Lower hybrid waves can be seen up to 3 perpendicular wavelengths away from

striation boundary. This does not agree with the model which predicts that the lower hybrid wave energy should be confined to radiate within the group velocity angle for this mode (~3.5°) and, thus, should only extend about half a perpendicular wavelength from the boundary. The discrepancy may arise from the fact that the striation boundary has a density gradient scale length on the order of the lower hybrid wavelength and is, thus, not a sharp interface, as assumed in the model, as far as the lower hybrid modes are concerned.

The relative amplitudes of the various wave modes may be summarized as follows. The amplitude of the parallel magnetic field, $B_z$, component of the reflected whistler wave is typically 80% of the incident wave. The $B_z$ component amplitude of the reflected lower hybrid wave is typically 15% of the incident whistler, reaching a maximum of 26%. The transmitted lower hybrid, on the other hand, is rather insignificant having a relative $B_z$ amplitude of only 3%. We further calculate that the reflected lower hybrid wave energy density is typically 10%, and reaches a maximum of 31%, of the incident whistler energy density. The lower hybrid, compared to the whistler wave, has a larger proportion of the wave energy contained in the perpendicular electric field, $E_x$, component. When we make the comparison in terms of $E_x$, we find the reflected lower hybrid wave amplitude to be typically 71%, reaching a maximum of 122%, of the incident whistler. These relative amplitudes are very similar to what has been observed by Bell and coworkers in experiments involving whistler waves launched into striated regions of the ionosphere, mode-converting to lower hybrid waves. Their data show that the mode-converted lower hybrid $E_x$ amplitude is normally on the order of incident whistler $E_x$. From this correspondence between the relative $E_x$ amplitudes found in the lab and in the ionosphere, we conclude

that in these experiments the mode-conversion actually occurs at the density striations via the linear mode-coupling mechanism.

Finally, we calculate that mode-conversion of naturally occurring whistler waves, if it happens as in the laboratory, should produce typical lower hybrid wave electric field amplitudes over an order of magnitude smaller than observed. This discrepancy may indicate that the mode-conversion process in the ionosphere is much more efficient than observed in the lab, or that it can only account for a small fraction of the observed wave amplitude. Thus, while the mode-conversion process may not be the primary source for lower hybrid waves associated with striations, it can not be ruled out as a possible source of some of the observed waves.

## Acknowledgments

This work has benefited greatly from the efforts and contributions of each of the members of the LAPD laboratory, and we would particularly like to acknowledge the stalwart efforts of A. Burke, S. Rosenberg, T. Tisdale, and S. Vincena in the arduous task of acquiring the data. The research is supported by ONR grant #N0001491J1172.

## References

Al'pert, Y., 40 years of whistlers, *J. Atmos. Terr. Phys., 42*, 1, 1980.

Al'pert, Y., *The near earth and interplanetary plasma*, vols. 1 and 2, Cambridge University Press, Cambridge, 1983.

Bell, T. F. and H. D. Ngo, Electrostatic waves stimulated by coherent VLF signals propagating in and near the inner radiation belt, *J. Geophys. Res., 93*, 2599, 1988.

Bell, T. F. and H. D. Ngo, Electrostatic lower hybrid waves excited by electromagnetic whistler mode waves scattering from planar magnetic-field-aligned plasma density irregularities, *J. Geophys. Res., 95*, 149, 1990.

Bell, T. F., H. G. James, U. S. Inan, and J. P. Katsufrakis, The apparent spectral broadening of VLF transmitter signals during transionospheric propagation, *J. Geophys. Res., 88*, 4813, 1983.

Carpenter, D. L., Ducted whistler-mode propagation in the magnetosphere; a half-gyrofrequency upper intensity cutoff and some associated wave growth phenomena, *J. Geophys. Res., 73*, 2919, 1968.

Carpenter, D. L., Some aspects of plasmapause probing by whistlers, *Radio Sci., 18*, 917, 1983.

Cerisier, J. C., Ducted and partly ducted propagation of VLF waves through the magnetosphere, *J. Atmos. Terr. Phys., 36*, 1443, 1974.

Chang, T., Lower-hybrid collapse, caviton turbulence, and charged particle energization in the topside auroral ionosphere and magnetosphere, *Phys. Fluids B, 5*, 2646, 1993.

Chen, F. F., Electric probes, *Plasma Diagnostic Techniques*, eds. R. H. Huddlestone and S. L. Leonard, Academic Press, New York, 113, 1965.

Clark, D. H. and W. J. Raitt, The global morphology of irregularities in the topside ionosphere as measured by the total ion current probe on ESRO-4, *Planet Space Sci., 24*, 873, 1976.

Dyson, P. L., Direct measurements of the size and amplitude of irregularities in the topside ionosphere, *J. Geophys. Res., 74*, 6291, 1969.

Fejer, B. G. and M. C. Kelley, Ionospheric irregularities, *Rev. Geophys. Space Phys., 18*, 401, 1980.

Gallet, R. M., J. M. Richardson, B. Wieder, G. B. Ward, and B. N. Harding, Microwave whistler mode propagation in a dense laboratory, *Phys. Rev. Lett., 4*, 347, 1960.

Garbe, G. P., R. L. Arnoldy, T. E. Moore, P. M. Kintner, and J. L. Vago, Observations of transverse ion acceleration in the topside ionosphere, *J. Geophys. Res., 97*, 1257, 1992.

Gekelman, W., H. Pfister, Z. Lucky, J. Bamber, D. Leneman, and J. Maggs, Design, construction, and properties of the Large Plasma Device — the LAPD at UCLA, *Rev. Sci. Instrum., 62*, 2875, 1991.

Helliwell, R. A., *Whistlers and Related Ionospheric Phenomena*, Stanford University Press, Stanford, 1965.

Herman, J. R., Spread F and ionospheric F region irregularities, *Rev. Geophys.*, *4*, 255, 1966.

Jackson, J. D., *Classical Electrodynamics*, John Wiley and Sons, New York, 1975.

James, H. G., Wave propagation experiments at medium frequencies between two ionospheric satellites, 2, Whistler-mode pulses, *Radio Sci.*, *13*, 543, 1978.

James, H. G. and T. F. Bell, Spin modulation of spectrally broadened VLF signals, *J. Geophys. Res.*, *92*, 7560, 1987.

Kelley, M. C. and F. S. Mozer, A satellite survey of vector electric fields in the ionosphere at frequencies of 10-500 Hz, 1, Isotropic, high-latitude electrostatic emissions, *J. Geophys. Res.*, *77*, 4158, 1972.

Kintner, P. M., J. Vago, S. Chesney, R. L. Arnoldy, K. A. Lynch, C. J. Pollock, and T. E. Moore, Localized lower hybrid acceleration of ionospheric plasma, *Phys. Rev. Lett.*, *68*, 2448, 1992.

Lovberg, R. H., Magnetic probes, *Plasma Diagnostic Techniques*, eds. R. H. Huddlestone and S. L. Leonard, Academic Press, New York, 69, 1965.

Maggs, J. E., Nonlinear evolution of the auroral electron beam, *J. Geophys. Res.*, *94*, 3631, 1989.

Pfister, H., W. Gekelman, J. Bamber, D. Leneman, and Z. Lucky, A fully three-dimensional-movable, 10-m-long, remotely controllable probe drive for a plasma discharge device, *Rev. Sci. Instrum.*, *62*, 2884, 1991.

Piliya, A. D., Wave conversion in an inhomogeneous plasma, *Sov. Phys. Tech. Phys.*, *11*, 609, 1966.

Shawhan, S. D., Magnetospheric plasma waves, *Solar System Plasma Physics, vol. III*, eds. C. F. Kennel, L. J. Lanzerotti, and E. N. Parker, 211, 1979.

Shawhan, S. D. and D. A. Gurnett, VLF electric and magnetic fields observed with the Javelin 8.45 sounding rocket, *J. Geophys. Res., 73*, 5649, 1968.

Singh, N., Ponderomotive versus mirror force in creation of the filamentary cavities in auroral plasma, *Geophys. Res. Lett., 21*, 257, 1994.

Smith, R. L. and J. J. Angerami, Magnetospheric properties deduced from OGO 1 observations of ducted and nonducted whistlers, *J. Geophys. Res., 73*, 1, 1968.

Stenzel, R. L., Self-ducting of large-amplitude whistler waves, *Phys. Rev. Lett.* **35**, 574 (1975).

Stenzel, R. L., Whistler wave propagation in a large magnetoplasma, *Phys. Fluids, 19*, 857, 1976a.

Stenzel, R. L., Filamentation instability of a large amplitude whistler wave, *Phys. Fluids, 19*, 865, 1976b.

Stenzel, R. L., Antenna radiation patterns in the whistler wave regime measured in a large laboratory plasma, *Radio Science, 11*, 1045, 1976c.

Stenzel, R. L. and W. Gekelman, Electrostatic waves near the lower hybrid frequency, *Phys. Rev. A, 11*, 2057, 1975.

Stix, T. H., *The Theory of Plasma Waves*, McGraw-Hill Book Company, New York, 1962.

Sugai, H., M. Maruyama, M. Sato, and S. Takeda, Whistler wave ducting caused by antenna actions, *Phys. Fluids, 21*, 690, 1978a.

Sugai, H., M. Sato, K. Ido, and S. Takeda, Dispersion and attenuation of whistler waves in a finite plasma, *J. Phys. Soc. Japan*, *44*, 1953, 1978b.

Sugai, H., K. Ido, H. Niki, S. Takeda, and K. Mima, Whistler wave trapping in a narrow density trough, *J. Phys Soc. Japan*, *46*, 1647, 1979.

Sugai, H., H. Niki, and S. Takeda, Whistler wave trapping in a density crest, *Phys. Fluids, 23*, 2134, 1980.

Vago, J. L., P. M. Kintner, S. W. Chesney, R. L. Arnoldy, K. A. Lynch, T. E. Moore, and C. J. Pollock, Transverse ion acceleration by localized lower hybrid waves in the topside ionosphere, *J. Geophys. Res.*, *97*, 16935, 1992.

Walker, A. D. M., The theory of whistler propagation, *Revs. Geophys. Space Phys.*, *14*, 629, 1976.